

Local likelihood estimation of complex tail dependence structures in high dimensions, applied to U.S. precipitation extremes

Daniela Castro Camilo¹ and Raphaël Huser¹

June 15, 2022

Abstract

In order to model the complex non-stationary dependence structure of precipitation extremes over the entire contiguous U.S., we propose a flexible local approach based on factor copula models. Our sub-asymptotic spatial modeling framework yields non-trivial tail dependence structures, with a weakening dependence strength as events become more extreme, a feature commonly observed with precipitation data but not accounted for in classical asymptotic extreme-value models. To estimate the local extremal behavior, we fit the proposed model in small regional neighborhoods to high threshold exceedances, under the assumption of local stationarity. This allows us to gain in flexibility, while making inference for such a large and complex dataset feasible. Adopting a local censored likelihood approach, inference is made on a fine spatial grid, and local estimation is performed taking advantage of distributed computing resources and of the embarrassingly parallel nature of this estimation procedure. The local model is efficiently fitted at all grid points, and uncertainty is measured using a block bootstrap procedure. An extensive simulation study shows that our approach is able to adequately capture complex, non-stationary dependencies, while our study of U.S. winter precipitation data reveals interesting differences in local tail structures over space, which has important implications on regional risk assessment of extreme precipitation events. A comparison between past and current data suggests that extremes in certain areas might be slightly wider in extent nowadays than during the first half of the twentieth century.

Keywords: climate change, factor copula model, local likelihood, non-stationarity, spatial extreme, threshold exceedance.

¹Computer, Electrical and Mathematical Sciences and Engineering (CEMSE) Division, King Abdullah University of Science and Technology (KAUST), Thuwal 23955-6900, Saudi Arabia. E-mails: daniela.castro@kaust.edu.sa, raphael.huser@kaust.edu.sa

1 Introduction

Water-related extremes such as floods and droughts can heavily impact human life, affecting our society, economic stability, and environmental sustainability. In recent years, we have witnessed an acceleration of the water cycle in some areas of the globe, including an increase in the frequency and intensity of heavy precipitation, sadly illustrated with a number of unprecedented hurricane events that recently hit the Caribbean islands and the Southeastern United States (U.S.) in August–September, 2017. These climate changes have motivated the development of stochastic models for risk assessment and uncertainty quantification of extreme weather events. In the univariate context, the generalized extreme-value distribution with time-varying parameters has been used to study the effect of climate change on global precipitation annual maxima (Westra *et al.*, 2013). More recently, Fischer and Knutti (2016) have adopted an empirical approach to study heavy rainfall intensification, validating the theory predicted by early generations of general circulation models. Similarly, Hoerling *et al.* (2016) analyzed trends in U.S. heavy precipitation data. Beyond the univariate context, several studies have focused on the spatial or spatio-temporal modeling of precipitation extremes within and across different catchments (Cooley *et al.*, 2007; Thibaud *et al.*, 2013; Huser and Davison, 2014), leading to extreme river discharges (Asadi *et al.*, 2015) or on the risk of heavy snowfall in mountainous areas (Blanchet and Davison, 2011). In these small regions, however, the spatial dependence structure is often assumed to be stationary. By contrast, in this paper we focus on modeling the complex, non-stationary, spatial dependence structure of U.S. winter precipitation extremes on a continental scale, and we study whether or not it might have changed over the past century.

Assessing the behavior of extreme events over space entails many challenges. First, data are measured at a finite number of locations, but extrapolation is typically required at any other location of the study region. In our case, the study region is the contiguous U.S. and

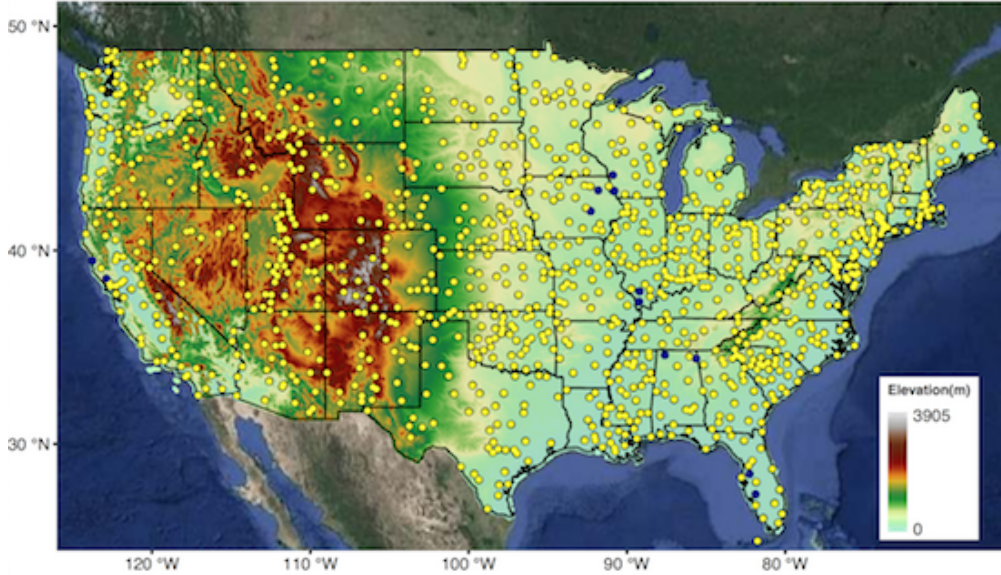


Figure 1: Topographic map of the contiguous U.S. with the 1218 weather stations (dots). Blue dots represent the stations chosen below to illustrate the results.

the monitoring stations at which data are collected are displayed in Figure 1. Second, by contrast with classical geostatistics where the estimation target is usually the (conditional) mean, statistics of extremes focuses on high (or low) quantiles and extrapolation is not only required over space, but also into the joint upper (or lower) tail of the distribution. Third, the scarcity of extremes results in uncertainty inflation, especially when very high quantiles have to be estimated, and thus it is important to develop efficient inference methods that can potentially be applied in high dimensions. Finally, a recurrent problem with large heterogeneous regions, such as the contiguous U.S., is the modeling of spatial non-stationarity. This may concern both marginal distributions and the dependence structure. As pointed out by [Huser and Genton \(2016\)](#), misspecification of the joint distribution of extremes may result in poor estimation of spatial risk measures. There is no universal consensus on how to handle non-stationarity; however, it is often both useful and realistic to assume some weak form of local stationarity. In this work, we fit a very flexible non-stationary, but locally stationary, spatial model to U.S. winter precipitation extremes, which contrasts with the quite rigid fully parametric model fitted by [Huser and Genton \(2016\)](#), and the non-parametric

approach adopted by [Castro Camilo and de Carvalho \(2016\)](#), whereby a family of bivariate extreme-value dependence structures at different sites are linked through a smooth function of covariates, while neglecting spatial dependence. The literature on spatial extremes is mostly divided into two mainstream approaches: the first approach defines extreme events as block (e.g., annual) maxima, which are typically modeled using max-stable processes ([Wes- tra and Sisson, 2011](#); [Davison and Gholamrezaee, 2012](#); [Huser and Genton, 2016](#)); the latter can be regarded as the functional generalization of multivariate extreme-value distributions, and they arise as natural limits of properly renormalized maxima of random fields. The second approach defines extreme events as high threshold exceedances, which are usually modeled using generalized Pareto processes, i.e., the threshold counterpart of max-stable processes ([Ferreira and de Haan, 2014](#); [Thibaud and Opitz, 2015](#); [de Fondeville and Davi- son, 2016](#)). Both max-stable and generalized Pareto processes are “ultimate” models, in the sense that they have an asymptotic characterization for block maxima and threshold ex- ceedances, respectively. However, their tail dependence structure is fairly rigid: max-stable copulas are invariant to the operation of taking componentwise maxima, while generalized Pareto copulas are invariant to thresholding at higher levels. This lack of tail flexibility has re- cently motivated the development of “penultimate” spatial models for threshold exceedances ([Wadsworth and Tawn, 2012](#); [Opitz, 2016](#); [Huser *et al.*, 2017](#); [Huser and Wadsworth, 2017](#)), which, unlike ultimate models, can capture weakening extremal dependence strength on the way to their limiting generalized Pareto process. To illustrate this important issue, [Figure 2](#) shows, for a range of quantiles $u \in [0.95, 0.999]$, the conditional probability

$$\chi_h(u) = \Pr\{Y_1 > F_1^{-1}(u) \mid Y_2 > F_2^{-1}(u)\}, \quad Y_j = Y(\mathbf{s}_j) \sim F_j, \quad j = 1, 2, \quad (1.1)$$

estimated for six selected pairs of stations $\{\mathbf{s}_1, \mathbf{s}_2\} \subset \mathcal{S}$ at distance $h = \|\mathbf{s}_1 - \mathbf{s}_2\|$, where $Y(\mathbf{s})$, $\mathbf{s} \in \mathcal{S}$, denotes the 5 day-cumulative winter precipitation random field defined over the contiguous U.S. (denoted \mathcal{S}). While the function $\chi_h(u)$ in [\(1.1\)](#) appears to be decreasing as

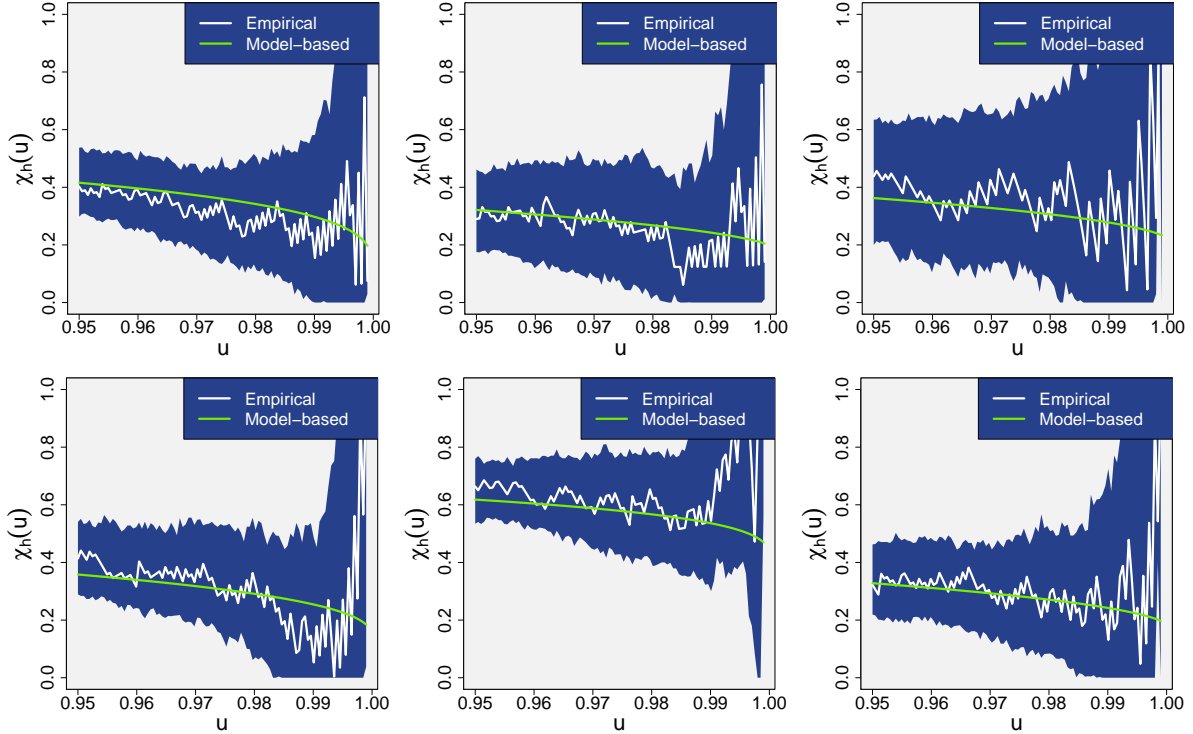


Figure 2: Empirical (white) and model-based (green) estimates for $\chi_h(u)$ as a function of the threshold $u \in [0.95, 0.999]$ for six selected pairs of stations in California at $h = 125\text{km}$ apart (top left), Iowa at $h = 114\text{km}$ apart (top middle), Wisconsin at $h = 60\text{km}$ apart (top right), Alabama at $h = 183\text{km}$ apart (bottom left), Illinois at $h = 57\text{km}$ apart (bottom middle), and Florida at $h = 130\text{km}$ apart (bottom right). Confidence envelopes for the empirical estimates (dark blue) are based on 300 block bootstrap samples with monthly blocks. Details on the fitted model are given in Sections 2 and 5.

a function of u for some pairs of stations, a generalized Pareto process *always* assumes that $\chi_h(u) \equiv \chi_h$ is constant in u (Rootzén *et al.*, 2017), hence potentially leading to significant overestimation of the dependence strength at higher quantiles. In Section 2, we develop a non-stationary model capturing non-trivial tail dependence, i.e., allowing for a positive limit $\chi_h = \lim_{u \rightarrow 1} \chi_h(u) > 0$, while at the same time having a decreasing $\chi_h(u)$ function with known limiting extreme-value dependence structure. Our non-stationary model builds upon the stationary exponential factor copula model proposed by Krupskii *et al.* (2016), which has attractive modeling features, and is computationally more convenient than the models proposed by Huser *et al.* (2017) and Huser and Wadsworth (2017). It fundamentally differs from the Laplace model of Opitz (2016), which strongly focuses on capturing tail

independence ($\chi_h = 0$) and the decay rate towards the limit, rather than tail dependence ($\chi_h > 0$), which is the type of extremal behavior suggested by our precipitation data at small scales (or at least, $\chi_h(u) > 0$ for quite high thresholds u); recall Figure 2.

Inference for extreme-value models is known to be particularly cumbersome. When max-stable processes are directly or indirectly involved, the likelihood function becomes excessively prohibitive to compute in moderate to large dimensions (Castruccio *et al.*, 2016), and this has led to the use of less efficient composite likelihood approaches (Padoan *et al.*, 2010; Westra and Sisson, 2011; Huser and Davison, 2013; Thibaud *et al.*, 2013; Huser and Davison, 2014). Alternatively, threshold approaches lead to simpler, significantly less demanding likelihoods, although their routine application to high-dimensional datasets is hampered by the need to censor observations involving non-extreme data (i.e., below a high threshold), which entails expensive multidimensional integrals; see, e.g., Wadsworth and Tawn (2014), Thibaud and Opitz (2015), Huser *et al.* (2017) and Huser and Wadsworth (2017). Other censoring schemes have been investigated by Engelke *et al.* (2015) and Opitz (2016), but they cause bias (Huser *et al.*, 2016). More recently, Morris *et al.* (2017) impute the censored, non-extreme, observations using a simulation-based algorithm within a Bayesian framework. In this work, although our full dataset comprises 1218 monitoring stations over the U.S., the dimensionality is considerably reduced by adopting a local estimation approach, making it possible to perform traditional censored likelihood inference in a robust and efficient way.

In Section 2, the stationary exponential factor copula model and a non-stationary generalization are presented, and their tail properties are studied. Section 3 discusses censored local likelihood inference based on high threshold exceedances. In Section 4, a simulation study is conducted to assess the performance of our approach in various non-stationary contexts. In Section 5, we apply this model to study the dependence structure of heavy precipitation data over the whole contiguous U.S., and we perform a subsequent comparison

analysis between various subperiods to determine whether or not the extremal dependence strength has changed over the past century, and if so, where changes might have occurred. Section 6 concludes with some discussion.

2 Modeling spatial extremes using factor copulas

2.1 Copula models

A copula is a multivariate probability distribution with $\text{Unif}(0, 1)$ margins. Copulas are used to describe the dependence between random variables, and may be used to link univariate marginal distributions to construct a joint distribution. Specifically, let $(X_1, \dots, X_D)^T \in \mathbb{R}^D$ be a random vector with continuous marginals $F_j(x) = \Pr(X_j \leq x)$, $j = 1, \dots, D$. The copula of $(X_1, \dots, X_D)^T$ is defined through the (uniform) random vector $(U_1, \dots, U_D)^T = \{F_1(X_1), \dots, F_D(X_D)\}^T$ as $C(u_1, \dots, u_D) = \Pr(U_1 \leq u_1, \dots, U_D \leq u_D)$. Sklar (1959) showed that each multivariate distribution $F(x_1, \dots, x_D)$ with continuous margins $F_j(x)$ has a unique copula C , which may be expressed as

$$F(x_1, \dots, x_D) = C\{F_1(x_1), \dots, F_D(x_D)\} \iff C(u_1, \dots, u_D) = F\{F_1^{-1}(u_1), \dots, F_D^{-1}(u_D)\}; \quad (2.1)$$

this motivates a two-step approach for inference, where margins are treated separately from the dependence structure. Based on (2.1), several copula families have been proposed and applied in practice for the modeling of environmental data, the most common one being the Gaussian copula obtained by choosing the joint distribution F to be the standard multivariate Gaussian distribution $\Phi_D(\cdot; \Sigma)$ with some correlation matrix Σ . Other more flexible elliptical copulas may be derived similarly, such as the Student- t copula, which is tail-dependent as opposed to the Gaussian copula. An alternative general family of copulas generating interesting tail dependence structures are factor copula models (Krupskii and Joe, 2015; Krupskii *et al.*, 2016), in which a random and unobserved factor affects all measurements simultaneously. In Section 2.2, we describe the construction of the stationary exponential factor copula model

proposed by Krupskii *et al.* (2016), which has appealing modeling and inference properties, and we then embed it in a more general non-stationary model in Section 2.3.

2.2 The stationary exponential factor copula model

Let $Z(\mathbf{s})$, $\mathbf{s} \in \mathcal{S} \subset \mathbb{R}^2$, be a standard Gaussian process with stationary correlation function $\rho(h)$ (see Gneiting *et al.* (2006) for a review of correlation functions), and let $V \geq 0$ be an exponentially distributed random variable with rate parameter $\lambda > 0$, independent of $Z(\mathbf{s})$, and which does not depend on the spatial location $\mathbf{s} \in \mathcal{S}$. The exponential factor copula model may be expressed in continuous space through the random process

$$W(\mathbf{s}) = Z(\mathbf{s}) + V, \quad \mathbf{s} \in \mathcal{S}. \quad (2.2)$$

The W process in (2.2) is essentially a Gaussian *location* mixture, i.e., a standard Gaussian process with a random, exponentially distributed, constant mean. In this sense, it has similarities with the Student- t process, which can be viewed as a Gaussian *scale* mixture (with standard deviation following a specific inverse gamma distribution). However, both models are not nested in each other, and their dependence structures have significant dissimilarities.

Notice that although Model (2.2) may seem quite artificial, it is only used to generate a flexible upper tail dependence structure, which we then fit to precipitation extremes. In other words, we disregard the margins and only consider the copula associated to (2.2), which we fit to high threshold exceedances using a censored likelihood approach, reducing the contribution of small precipitation values; more details are given in Sections 3 and 5.

From (2.2), each configuration of D sites $\{\mathbf{s}_1, \dots, \mathbf{s}_D\} \subset \mathcal{S}$ yields a D -variate copula as follows: let $Z_j = Z(\mathbf{s}_j)$ and $W_j = W(\mathbf{s}_j)$, $j = 1, \dots, D$. The random vector $\mathbf{Z} = (Z_1, \dots, Z_D)^T$ has a multivariate normal distribution with correlation matrix $\Sigma_{\mathbf{Z}}$ that depends on the correlation function $\rho(h)$ and the sites' configuration, i.e., $\mathbf{Z} \sim \Phi_D(\cdot; \Sigma_{\mathbf{Z}})$. The components of the random vector $\mathbf{W} = (W_1, \dots, W_D)^T$ are $W_j = Z_j + V$, $j = 1, \dots, D$, where $V \sim \text{Exp}(\lambda)$

is independent of \mathbf{Z} ; by conditioning on V , the joint distribution of \mathbf{W} may be expressed as

$$F_D^{\mathbf{W}}(w_1, \dots, w_D) = \lambda \int_0^\infty \Phi_D(w_1 - v, \dots, w_D - v; \boldsymbol{\Sigma}_{\mathbf{Z}}) \exp(-\lambda v) dv, \quad (2.3)$$

whilst its density is

$$f_D^{\mathbf{W}}(w_1, \dots, w_D) = \lambda \int_0^\infty \phi_D(w_1 - v, \dots, w_D - v; \boldsymbol{\Sigma}_{\mathbf{Z}}) \exp(-\lambda v) dv, \quad (2.4)$$

where $\phi_D(\cdot; \boldsymbol{\Sigma})$ is the multivariate standard normal density with correlation matrix $\boldsymbol{\Sigma}$. Simpler expressions avoiding the univariate integral in (2.3) and (2.4) can be obtained; see Appendix A. Applying (2.1), the resulting copula and its density may be written as

$$C_D^{\mathbf{W}}(u_1, \dots, u_D) = F_D^{\mathbf{W}}(w_1^*, \dots, w_D^*), \quad c_D^{\mathbf{W}}(u_1, \dots, u_D) = \frac{f_D^{\mathbf{W}}(w_1^*, \dots, w_D^*)}{\prod_{j=1}^D f_1^{\mathbf{W}}(w_j^*)}, \quad (2.5)$$

where $w_j^* = (F_1^{\mathbf{W}})^{-1}(u_j; \lambda)$, $j = 1, \dots, D$, and $F_1^{\mathbf{W}}(\cdot; \lambda)$ and $f_1^{\mathbf{W}}(\cdot; \lambda)$ denote the marginal distribution and density of the W process, respectively. In particular, one can show that

$$F_1^{\mathbf{W}}(w; \lambda) = \Phi(w) - \exp(\lambda^2/2 - \lambda w)\Phi(w - \lambda), \quad (2.6)$$

where $\Phi(\cdot)$ is the standard normal distribution function; see (A.3) in Appendix A.

To illustrate the tail flexibility of the stationary exponential factor copula model, Figure 3 displays the function $\chi_h(u)$ defined in (1.1) as a function of the quantile level $u \in [0.95, 1]$ and the Euclidean distance $h = \|\mathbf{s}_1 - \mathbf{s}_2\| \geq 0$, for different rate $\lambda > 0$ and range $\delta > 0$ parameters, assuming an exponential correlation function $\rho(h) = \exp(-h/\delta)$, $h \geq 0$. While the range δ controls the correlation decay with distance, the rate λ determines the overall tail dependence strength and strongly impacts the value of $\chi_h(u)$ and χ_h at large distances, i.e., as $h \rightarrow \infty$. In particular, because the random factor V in (2.2) is common to all sites $\mathbf{s} \in \mathcal{S}$, spatial dependence in the W process does not vanish as $h \rightarrow \infty$. Therefore, this stationary model may be useful for (replicated) spatial data collected on a local or regional scale, but it might not be realistic on larger scales, such as the whole continental U.S.; Section 2.3

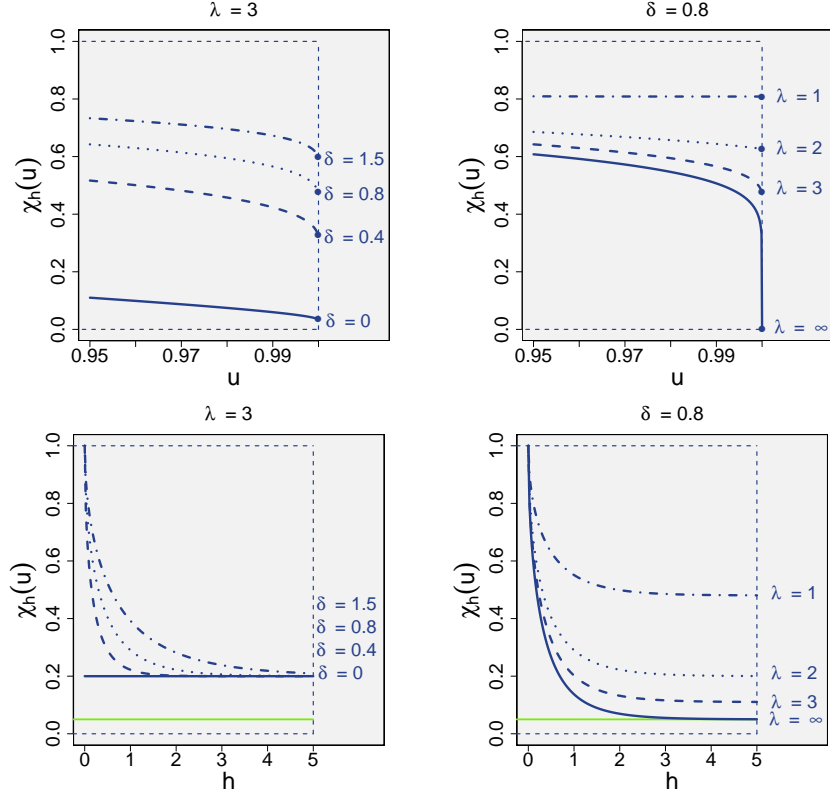


Figure 3: Conditional probability $\chi_h(u)$ as defined in (1.1) for the stationary exponential factor model with rate parameter $\lambda > 0$ and exponential correlation function $\rho(h) = \exp(-h/\delta)$, plotted with respect to the level $u \in [0.95, 1]$ at distance 0.1 (top) and with respect to the distance $h \in [0, 5]$ for fixed $u = 0.95$ (bottom). Left: fixed $\lambda = 3$ and $\delta = 0, 0.4, 0.8, 1.5$. Right: fixed $\delta = 0.8$ and $\lambda = 1, 2, 3, \infty$. The dots in the top panels correspond to the limit $\chi_h = \lim_{u \rightarrow 1} \chi_h(u)$, and the green horizontal line in the bottom panels corresponds to perfect independence.

discusses a flexible extension to capture non-stationary tail dependencies on larger regions. As shown by Krupskii *et al.* (2016), the distribution of the random factor characterizes the tail properties of the copula (2.5); in particular, the stationary exponential factor copula model is tail-dependent (i.e., $\chi_h > 0$) for fixed $\lambda > 0$, and its upper-tail dependence structure is governed the Hüsler and Reiss (1989) copula, which has been widely used for multivariate and spatial extremes (Davison *et al.*, 2012). Moreover, as $\lambda \rightarrow \infty$, Model (2.2) boils down to the Gaussian copula, which is tail-independent (i.e., $\chi_h = 0$). Conversely, as $\lambda \rightarrow 0$, the W process is perfectly dependent over space. Thus, the exponential factor copula model interpolates between tail independence as $\lambda \rightarrow \infty$ and perfect dependence as $\lambda \rightarrow 0$, while capturing a wide range of non-trivial tail dependence structures for $\lambda \in (0, \infty)$.

We now provide more detailed information on the sub-asymptotic behavior of Model (2.2), refining the description of its tail structure. The rate at which $\chi_h(u)$ converges to χ_h , as $u \rightarrow 1$, characterizes the flexibility of the process to capture sub-asymptotic extremal dependence. In practice, this is important, as the model will always be fitted at a finite threshold. Proposition 1 shows that this rate of convergence is regulated by the parameter λ ; the smaller λ the faster the convergence, and vice versa. The proof is deferred to Appendix B.

Proposition 1. *Consider Model (2.2) with rate $0 < \lambda < \infty$. One has the expansion*

$$\chi_h(u) - \chi_h = -f(u) + (2 - \chi_h) \{ \lambda s(u) + k(u) \} \{ 1 + o(1) \}, \quad u \rightarrow 1,$$

where $f(u) \sim \frac{2\phi\{z(u)\}}{(1-u)z(u)}$, $s(u) \sim \frac{\phi\{z(u)\}}{(1-u)z(u)\{z(u)-\lambda\}}$ and, for $0 < \rho(h) < 1$, $k(u) \sim \frac{2\phi\{z(u)-\lambda\}}{(2-\chi_h)\{z(u)-\lambda\}}$, with $z(u) = (F_1^{\mathbf{W}})^{-1}(u; \lambda) \sim -\lambda^{-1} \log(1-u) + \lambda/2\{1 + o(1)\}$ such that in the limit as $u \rightarrow 1$,

$$\chi_h(u) - \chi_h = -f(u)\{1 + o(1)\}.$$

Other types of tail dependence structures can be obtained using alternative distributions for the random factor V (see Krupskii *et al.*, 2016), but we here restrict ourselves to the exponential factor copula model, which yields flexible tail structures and fast inference.

2.3 A non-stationary exponential factor copula model

The assumption of stationarity underlying (2.2) is unrealistic over large heterogeneous regions, such as the whole U.S., but it may be the starting point for more sophisticated models; in particular, the true precipitation data generating process might be approximately stationary in small regions, providing support for non-stationary, but locally stationary, models.

We here assume that Model (2.2) provides a good approximation to the local tail dependence structure, while stemming from a more complex global data generating process. To make sure that the local stationary model (2.2) can truly come from a well-defined global

stochastic process, we now describe one possible way to embed it into a non-stationary process. Our proposed model extension, equivalent to (2.2) on infinitesimal regions, is

$$W(\mathbf{s}) = Z(\mathbf{s}) + \lambda_{\mathbf{s}}^{-1}E, \quad \mathbf{s} \in \mathcal{S}, \quad (2.7)$$

where $Z(\mathbf{s})$ is a zero mean Gaussian process with non-stationary correlation function $\rho(\mathbf{s}_1, \mathbf{s}_2)$ and E is a standard exponentially distributed common factor, independent of $Z(\mathbf{s})$. The rate parameter $\lambda_{\mathbf{s}} > 0$, $\mathbf{s} \in \mathcal{S}$, is assumed to be a smooth surface, which dictates different degrees of tail dependence in distinct regions. Although (2.7) may not realistically capture long-distance dependencies owing to the latent factor E being constant over space, its estimated spatially-varying parameters provide relevant information about the local dependence structure; Model (2.7) is therefore useful to “think” about the results *globally*, while providing an accurate description of the extremal dependence structure *locally* (or *regionally*). A more realistic global model might be obtained by replacing the random variable E by a slowly fluctuating latent process $E(\mathbf{s})$ with exponential margins, capturing the “between-region” dependence, but our local estimation approach would then lead to parameter identifiability issues if $E(\mathbf{s})$ is almost constant (i.e., highly dependent) within specific regions.

In the literature, different non-stationary correlation functions $\rho(\mathbf{s}_1, \mathbf{s}_2)$ have been proposed; see, e.g., Fuentes (2001), Nychka *et al.* (2002), Stein (2005), Paciorek and Schervish (2006), and Reich *et al.* (2011). Here, we focus on a non-stationary, locally isotropic, Matérn correlation function with constant smoothness parameter $\nu > 0$, constructed through the kernel convolution approach advocated by Paciorek and Schervish (2006); it is defined as

$$\rho(\mathbf{s}_1, \mathbf{s}_2) = \frac{2^{2-\nu} \delta_{\mathbf{s}_1} \delta_{\mathbf{s}_2}}{\Gamma(\nu) \{\delta_{\mathbf{s}_1}^2 + \delta_{\mathbf{s}_2}^2\}} \mathcal{K}_{\nu} \left(\frac{2\sqrt{2\nu}}{\sqrt{\delta_{\mathbf{s}_1}^2 + \delta_{\mathbf{s}_2}^2}} \|\mathbf{s}_1 - \mathbf{s}_2\| \right), \quad (2.8)$$

where $\delta_{\mathbf{s}} > 0$, $\mathbf{s} \in \mathcal{S}$, is a smoothly varying range parameter, $\Gamma(\cdot)$ is the Gamma function and \mathcal{K}_{ν} is the modified Bessel function of second kind of order ν . The stationary Matérn correlation function (obtained by setting $\delta_{\mathbf{s}} \equiv \delta$ for all $\mathbf{s} \in \mathcal{S}$) has become popular because

of its appealing properties (Stein, 1999). In particular, a Gaussian process with Matérn correlation function is m times mean-square differentiable if and only if $\nu > m$. For $\nu = 0.5$, it boils down to the exponential correlation function, which yields continuous but non-differentiable sample paths. As $\nu \rightarrow \infty$, sample paths are infinitely differentiable. The non-stationary correlation function defined in (2.8) is locally Matérn, and therefore it inherits these attractive properties. An extension of (2.8) allowing for varying degrees of smoothness over space has been proposed in the unpublished manuscript of Stein (2005) (see also Anderes and Stein (2011)), but in practice, estimating ν is cumbersome and conservative approaches are usually adopted. In our application in Section 5, ν is treated as constant over space.

Because the global model (2.7) is an extension of (2.2), they share similar types of tail dependence structures; this is summarized in Proposition 2. The proof, which extends the argument of Krupskii *et al.* (2016) to the non-stationary context, is deferred to Appendix B.

Proposition 2. *Consider the non-stationary model (2.7) with finite rate parameter $\lambda_{\mathbf{s}} > 0$. For all pairs of sites $\mathbf{s}_1, \mathbf{s}_2 \in \mathcal{S}$, the bivariate copula $C_2^{\mathbf{W}}(u_1, u_2)$ of $\{W(\mathbf{s}_1), W(\mathbf{s}_2)\}^T$ has limiting stable tail dependence function (see, e.g., Segers, 2012) given by*

$$\ell(x_1, x_2) = \lim_{q \rightarrow 0} \frac{1}{q} \{1 - C_2^{\mathbf{W}}(1 - qx_1, 1 - qx_2)\} = x_1 \Phi \left(\frac{\sqrt{\gamma_{12}}}{2} + \frac{\log(x_1/x_2)}{\sqrt{\gamma_{12}}} \right) + x_2 \Phi \left(\frac{\sqrt{\gamma_{12}}}{2} + \frac{\log(x_2/x_1)}{\sqrt{\gamma_{12}}} \right),$$

where $\gamma_{12} = \lambda_{\mathbf{s}_1}^2 - 2\rho(\mathbf{s}_1, \mathbf{s}_2)\lambda_{\mathbf{s}_1}\lambda_{\mathbf{s}_2} + \lambda_{\mathbf{s}_2}^2$, and $\Phi(\cdot)$ is the standard normal distribution function. In other words, Model (2.7) is in the max-domain of attraction of the non-stationary Brown-Resnick process (Kablichko *et al.*, 2009) with variogram γ_{12} , i.e., it is governed by the Hüsler and Reiss (1989) copula. Furthermore, Model (2.7) is tail-dependent and the limit $\chi_{12} = \lim_{u \rightarrow 1} \chi_{12}(u)$, with $\chi_{12}(u)$ defined analogously to (1.1) in the non-stationary context, is

$$\chi_{12} = 2 - \theta_2(\mathbf{s}_1, \mathbf{s}_2) = 2 - \ell(1, 1) = 2\{1 - \Phi(\sqrt{\gamma_{12}}/2)\} > 0. \quad (2.9)$$

The dependence measure $\theta_2(\mathbf{s}_1, \mathbf{s}_2) \in [1, 2]$ is called the bivariate extremal coefficient function of the associated limiting max-stable random field.

The extremal coefficient $\theta_2(\mathbf{s}_1, \mathbf{s}_2)$ implicitly defined in (2.9) encompasses the effects of all parameters involved in the model, i.e., $\lambda_{\mathbf{s}}, \delta_{\mathbf{s}}, \nu$, and we use it in our simulation experiments (Section 4) and the data application (Section 5) to study the performance of our model and to assess its ability to flexibly capture different levels of extremal dependence.

3 Local likelihood inference with partial censoring

Local likelihood estimation for univariate threshold exceedances was proposed by Davison and Ramesh (2000), while Anderes and Stein (2011) investigated how such an approach may be applied in the spatial context based on a single realization from a Gaussian process. We here detail how to perform local likelihood estimation based on high threshold exceedances by adapting the methodology developed by Anderes and Stein (2011) to the joint upper tail of the non-stationary copula model (2.7), under the assumption that its local stationary approximation (2.2) is valid in small regional neighborhoods. We assume that multiple replicates of the process are observed, with possibly arbitrary marginal distributions.

Since our focus is on the data’s dependence structure, we advocate a two-step semi-parametric estimation procedure, whereby margins are first estimated at each site separately using the empirical distribution function, and the copula model is then estimated locally in a second step by maximum likelihood, censoring low (i.e., non-extreme) values to prevent them from influencing the fit. Although more complex parametric approaches are also possible to estimate margins, we have found that the use of the rank-based empirical distribution function provides a robust and reliable method, which does not affect much the subsequent estimation of the copula. Such a two-step approach is standard in the copula literature, and has been studied in depth; see, e.g., Genest *et al.* (1995) and Joe (2014), Chapter 5.

The first step of our proposed estimation procedure consists in transforming the observed data non-parametrically to the uniform scale. Let y_{1j}, \dots, y_{Nj} denote N independent and

identically distributed observations at the j th monitoring station, with essentially arbitrary marginals. Pseudo-uniform scores may be obtained using ranks as follows:

$$u_{ij} = \frac{\text{rank}(y_{ij})}{N + 1}, \quad i = 1, \dots, N.$$

In the second step, the scores u_{ij} , $i = 1, \dots, N$, are treated as a perfect random sample from the $\text{Unif}(0, 1)$ distribution. To estimate the spatial copula structure, we then discretize the space \mathcal{S} (in our case, the whole contiguous U.S.) into a fine grid $\mathcal{G} \subset \mathcal{S}$. For each grid point $\mathbf{s}_0 \in \mathcal{G}$, we assume that the local stationary copula model (2.2) with parameters $\theta_0 = (\lambda_0, \delta_0, \nu_0)^T \in \Theta = (0, \infty)^3$, which stems from the global non-stationary model (2.7) with Matérn correlation (2.8), is valid in a small neighborhood $\mathcal{N}_{\mathbf{s}_0} \subset \mathcal{S}$ around \mathbf{s}_0 . In what follows, these regional neighborhoods will be determined by a small number, D_0 , of nearest stations from the site \mathbf{s}_0 , so we will write $\mathcal{N}_{\mathbf{s}_0} \equiv \mathcal{N}_{\mathbf{s}_0; D_0}$. Obviously, the choice of neighborhood is important: the stationary model (2.2) might be a poor approximation for large neighborhoods, whereas model fitting might be cumbersome for small neighborhoods characterized by a small number D_0 of stations. This bias-variance trade-off is tricky to deal with, and Section 5 describes one possible approach to mitigate this issue.

To estimate the local tail dependence structure, we suggest using a censored likelihood approach, which is standard in statistics for spatial extremes, though it has never been applied to Model (2.2); see, e.g., Ledford and Tawn (1996), Thibaud *et al.* (2013), Huser and Davison (2014), Wadsworth and Tawn (2014), Thibaud and Opitz (2015) and Huser *et al.* (2017). Essentially, vectors with non-extreme observations (i.e., lower than a high threshold) are partially or fully censored to prevent these low values from affecting the estimation of the extremal dependence structure. More precisely, for each grid point $\mathbf{s}_0 \in \mathcal{G}$ with associated neighborhood $\mathcal{N}_{\mathbf{s}_0; D_0}$, let $\mathbf{u}_j^0 = (u_{1j}^0, \dots, u_{Nj}^0)^T$, $j = 1, \dots, D_0$, denote the pseudo-uniform scores for each of the nearby stations in $\mathcal{N}_{\mathbf{s}_0; D_0}$, and let u_j^* , $j = 1, \dots, D_0$, be high marginal thresholds; in our application in Section 5, we take $u_j^* = 0.95$ for all j . Using the notation

introduced in (2.3)–(2.6), the censored local log-likelihood may be expressed as

$$\begin{aligned} \ell(\theta_0 | \mathcal{N}_{\mathbf{s}_0; D_0}) &= \sum_{i \in \mathcal{I}_{\text{nc}}} \log f_{D_0}^{\mathbf{W}}(w_{i1}^0, \dots, w_{iD_0}^0; \theta_0) - \sum_{i \in \mathcal{I}_{\text{nc}}} \sum_{j=1}^{D_0} \log f_1^{\mathbf{W}}(w_{ij}^0; \lambda_0) \\ &\quad + N_{\text{fc}} \times F_{D_0}^{\mathbf{W}}(w_1^*, \dots, w_{D_0}^*; \theta_0) + \sum_{i \in \mathcal{I}_{\text{pc}}} \log \partial_{J_i} F_{D_0}^{\mathbf{W}}(\max(w_{i1}^0, w_1^*), \dots, \max(w_{iD_0}^0, w_{D_0}^*); \theta_0), \end{aligned} \quad (3.1)$$

where $w_{ij}^0 = (F_1^{\mathbf{W}})^{-1}(u_{ij}^0; \lambda_0)$ and $w_j^* = (F_1^{\mathbf{W}})^{-1}(u_j^*; \lambda_0)$, $j = 1, \dots, D_0$, $\mathcal{I}_{\text{nc}} = \{i \in \{1, \dots, N\} : u_{ij} > u_j^*, \forall j = 1, \dots, D_0\}$ is the index set of all *non-censored* observations (i.e., all vector components are extreme), $\mathcal{I}_{\text{fc}} = \{i \in \{1, \dots, N\} : u_{ij} \leq u_j^*, \forall j = 1, \dots, D_0\}$ is the index set of all *fully censored* observations (i.e., none of the vector components are extreme) with $N_{\text{fc}} = |\mathcal{I}_{\text{fc}}|$, $\mathcal{I}_{\text{pc}} = \{1, \dots, N\} \setminus \{\mathcal{I}_{\text{nc}} \cup \mathcal{I}_{\text{fc}}\}$ is the index set of all *partially censored* observations (i.e., some, but not all, vector components are extreme), $J_i = \{j \in \{1, \dots, D_0\} : u_{ij} > u_j^*\}$ is the index set of threshold exceedances for the i th vector of observations, and ∂_{J_i} denotes differentiation with respect to the variables indexed by the set J_i . Numerical maximization of (3.1) yields the maximum likelihood estimates $\hat{\theta}_0 = (\hat{\lambda}_0, \hat{\delta}_0, \hat{\nu}_0)^T$ for location \mathbf{s}_0 . In Appendix A, we provide simple expressions for $f_{D_0}^{\mathbf{W}}$, $F_{D_0}^{\mathbf{W}}$ and $\partial_{J_i} F_{D_0}^{\mathbf{W}}$, which involve the D_0 -variate Gaussian density and the multivariate Gaussian distribution in dimension D_0 and $D_0 - |J_i|$, respectively. When D_0 is large, the computation of the multivariate Gaussian distribution can significantly slow down the estimation procedure. However, thanks to our local approach, D_0 is typically quite small, and this allows to estimate the model at a reasonable computational cost. Furthermore, because the likelihood maximizations can be done independently at each grid point $\mathbf{s}_0 \in \mathcal{G}$, we can easily take advantage of distributed computing resources to perform each fit in parallel.

Following Anderes and Stein (2011), it would also be possible to generalize (3.1) to obtain smoother parameter estimates over space. Specifically, one could instead maximize the weighted log-likelihood function defined as

$$\ell_\omega(\theta_0 | \mathcal{N}_{\mathbf{s}_0; D_0}) = \sum_{j=1}^{D_0} \omega(\|\mathbf{s}_j - \mathbf{s}_0\|) \{\ell(\theta_0 | \mathcal{N}_{\mathbf{s}_0; j}) - \ell(\theta_0 | \mathcal{N}_{\mathbf{s}_0; j-1})\}, \quad (3.2)$$

where $\omega(h) \geq 0$ is a non-negative weight function, and $\{\mathcal{N}_{\mathbf{s}_0;j}; j = 0, \dots, D_0\}$, denotes the nested sequence of subsets comprising the first j nearest neighbors of \mathbf{s}_0 , with the convention that $\mathcal{N}_{\mathbf{s}_0;0} = \emptyset$ and $\ell(\theta_0|\emptyset) = 0$. Choosing hard-thresholding weights with $\omega(\|\mathbf{s}_j - \mathbf{s}_0\|) = 1$ for all $\mathbf{s}_j \in \mathcal{N}_{\mathbf{s}_0;D_0}$ boils down to (3.1). However, smoother parameter estimates may be obtained by selecting soft-thresholding weights that smoothly decay to zero near the neighborhood boundaries, e.g., using the biweight function $\omega(h) = (1 - (h/\tau_0)^2)_+^2$, for some bandwidth $\tau_0 > 0$. Although this estimation approach seems quite appealing, it significantly increases the computational burden, since the weighted log-likelihood function (3.2) requires computing (3.1) D_0 times. For this reason, and because the censored likelihood procedure is already quite intensive, we do not pursue this approach further in this paper. Subsequent simulation and real data experiments are all based on (3.1).

4 Simulation study

4.1 Data-generating scenarios

In this section we study the flexibility of our global copula model (2.7) to describe complex extremal dynamics across space, and we assess the performance of our local estimation approach based on (3.1) at capturing such non-stationary dependence structures. We also analyze the sensitivity of the parameter estimates to the neighborhood size.

Data are simulated on a 25×25 grid in $\mathcal{S} = [1, 10]^2$ from the copula model stemming from (2.7) based on the non-stationary Matérn correlation function (2.8); 500 independent replicates are generated. We choose three different levels of smoothness by fixing $\nu = 0.5, 1.5, 2.5$, and we consider three scenarios for the range $\delta_{\mathbf{s}}$ and the rate $\lambda_{\mathbf{s}}$ parameters, representing various levels of non-stationarity in the tail behavior. The true parameter values and the bivariate extremal coefficient function (recall (2.9)) with respect to three different reference points, are shown in Figure 4 for the weakly, mildly and strongly non-stationary scenarios.

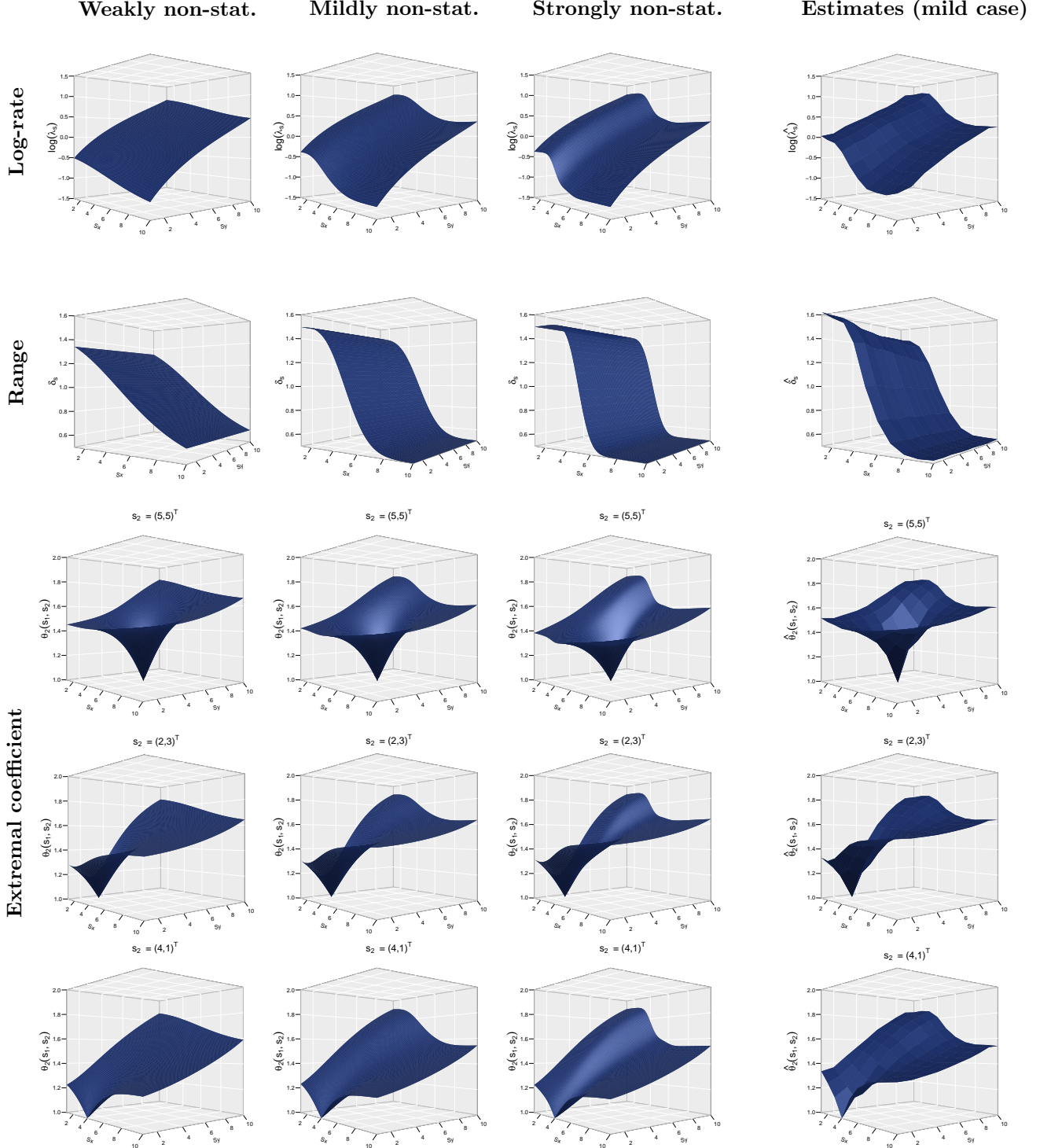


Figure 4: *Columns 1–3:* True spatially-varying log-rate $\log(\lambda_{\mathbf{s}})$ (1st row), range $\delta_{\mathbf{s}}$ (2nd row), and extremal coefficient $\theta_2(\mathbf{s}_1, \mathbf{s}_2)$ (3rd–5th rows) for a fixed location \mathbf{s}_2 . *Column 4:* Mean surface of estimated parameters for the mildly stationary scenario, based on 1000 simulation experiments, using the local censored likelihood approach with thresholds $u_j^* = 0.95$ for all j , and $D_0 = 20$ nearest neighbors, as detailed in Section 3. The smoothness parameter is fixed to $\nu = 2.5$.

4.2 Simulation results

In all simulations, the smoothness parameter ν is held fixed, while the rate $\lambda_{\mathbf{s}}$ and range $\delta_{\mathbf{s}}$ parameters are estimated on a 10×10 grid $\mathcal{G} \subset [1, 10]^2$ using the local estimation approach with censoring thresholds $u_j^* = 0.95$ for all j , as described in Section 3. To compute performance metrics and to measure the uncertainty of estimated parameters, we replicate all simulation experiments 1000 times.

We first detail the results for the mildly non-stationary scenario (second column of Figure 4) with $\nu = 2.5$ and choosing $D_0 = 20$ nearest neighbors, while results for the all simulation scenarios are summarized in Table 1. The rightmost column of Figure 4 displays mean surfaces, computed over the 1000 independent experiments, of the estimated log-rate $\log(\lambda_{\mathbf{s}})$ and range $\delta_{\mathbf{s}}$ parameters, as well as the fitted bivariate extremal coefficient functions for the three different reference locations. By comparing the true surfaces to the mean estimates, the bias appears to be quite small overall, except perhaps at the boundaries of the study region, \mathcal{S} . This is a well-known drawback of local estimation approaches: because the neighborhoods are asymmetric near the boundaries, the bias is generally more severe, and this can also be noticed in our case, e.g., in regions where $\theta_2(\mathbf{s}_1, \mathbf{s}_2) \approx 2$. This issue is similar to the boundary problem in kernel density estimation occurring with positively or compactly supported densities; some strategies have been advocated to deal with it, such as taking asymmetric kernels near the boundaries, or performing local linear regression (see, e.g., [Castro Camilo *et al.*, 2017](#)), but we do not pursue this here. Apart from this minor boundary problem, our local estimation approach succeeds in capturing the complex non-stationary dependence dynamics over space.

To assess the variability of the parameter estimates, Figure 5 displays a functional boxplot for the range parameter $\delta_{\mathbf{s}}$, projected onto the x -axis representing the only direction of variation in the true $\delta_{\mathbf{s}}$ values, and a surface boxplot for the bivariate extremal coefficient

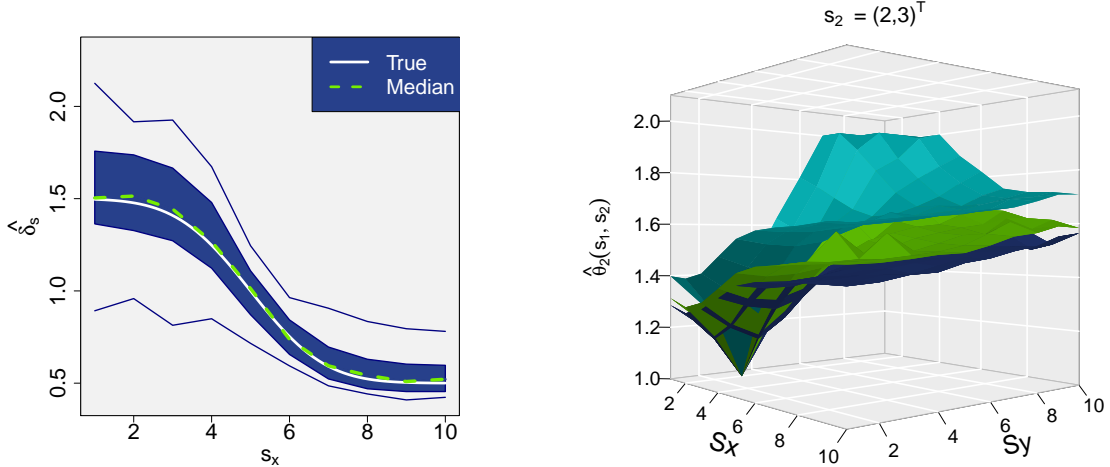


Figure 5: Functional boxplot (left) for the range $\delta_{\mathbf{s}}$, $\mathbf{s} = (s_x, s_y)^T$, plotted with respect to x -coordinate s_x , and surface boxplot (right) for the bivariate extremal coefficient $\theta_2(\mathbf{s}_1, \mathbf{s}_2)$, plotted as a function of location \mathbf{s}_1 for fixed $\mathbf{s}_2 = (2, 3)^T$. In the surface boxplot, the dark and light blue surfaces represent the 1st and 3rd quartiles (i.e., the “box” of the boxplot), respectively, while the green surface is the median. The surface boxplot’s “whiskers” are not displayed for better visualization. Both panels show the results for the mildly non-stationary case with $\nu = 2.5$ and $D_0 = 20$ nearest neighbors in the local estimation approach.

$\theta_2(\mathbf{s}_1, \mathbf{s}_2)$ for fixed $\mathbf{s}_2 = (2, 3)^T$. Functional and surface boxplots are the natural extensions of the classical boxplot to the case of functional data, and we refer to [Sun and Genton \(2012\)](#) and [Genton *et al.* \(2014\)](#) for their precise interpretation. As the true range parameter $\delta_{\mathbf{s}}$, $\mathbf{s} = (s_x, s_y)^T$, varies only with respect to s_x , it is easier to visualize its estimated uncertainty. As expected, $\delta_{\mathbf{s}}$ appears to be well estimated overall with higher uncertainty for larger $\delta_{\mathbf{s}}$ values. The estimated median curve follows the true curve very closely, even near the boundaries and around $s_x = 1$, where the true curve is the steepest, while the functional inter-quartile range is fairly narrow for all values of s_x . As for the extremal coefficient function, the surface boxplot suggests that it can also be rather well estimated with relatively low uncertainty. Table 1 reports the root mean integrated squared error (RMISE) for all the data generating configurations described in Section 4.1. The results are coherent with our intuition: the estimation is more difficult for higher levels of non-stationarity and rougher random fields (i.e., with smaller ν). Overall, simulations confirm that the non-stationary

Table 1: RMISEs for the rate $\hat{\lambda}_s$ and range $\hat{\delta}_s$ parameters for each smoothness parameter $\nu = 0.5, 1.5, 2.5$, computed over 1000 replicates from the data-generating configurations discussed in Section 4.1.

Configuration	$\nu = 0.5$		$\nu = 1.5$		$\nu = 2.5$	
	$\hat{\lambda}_s$	$\hat{\delta}_s$	$\hat{\lambda}_s$	$\hat{\delta}_s$	$\hat{\lambda}_s$	$\hat{\delta}_s$
Weakly non-stationary	0.09	0.59	0.03	0.01	0.03	0.00
Mildly non-stationary	0.09	0.69	0.06	0.02	0.04	0.00
Strongly non-stationary	0.17	0.89	0.15	0.05	0.22	0.02

factor copula model (2.7) is very flexible and is able to produce complex tail dependencies, and that our local censored estimation approach provides reasonable estimates of the true range and rate parameters, while capturing their dynamics over space.

To assess the performance of our local likelihood approach as a function of the neighborhood size, we fix the rate parameter λ_s to the strongly non-stationary scenario, while considering the weakly, mildly and strongly non-stationary cases for the range parameter δ_s (recall Figure 4), and we then fit the copula model using the local likelihood approach described in Section 3 with neighborhoods $\mathcal{N}_{s_0; D_0}$ defined in terms of $D_0 = 5, 10, 15, 20, 25$ nearest neighbors. Table 2 reports the RMISE for all cases. While the RMISE is quite small and fairly constant overall for the range δ_s , the rate λ_s seems more difficult to estimate, and it improves with lower degrees of non-stationarity for δ_s and bigger neighborhoods (i.e., with larger D_0), even in the strongly non-stationary scenario. This suggests that the size of neighborhoods will likely be dictated by available computational resources. Unless the non-stationarity is extremely severe, it is advisable to consider large neighborhoods, as this would improve the estimation efficiency at a fairly moderate cost in bias.

5 Case study: U.S. winter precipitation extremes

5.1 Data description

Daily precipitation data, freely available online, were gathered from the U.S. Historical Climatological Network (USHCN). They are measured in hundredth of an inch, and were

Table 2: RMISEs for the rate $\hat{\lambda}_s$ and range $\hat{\delta}_s$ parameters for $\nu = 2.5$, as a function of the number D_0 of nearest neighbors used in the local estimation approach. The rate $\hat{\lambda}_s$ was kept fixed to the strongly non-stationary case, while different degrees of non-stationarity are considered for the range $\hat{\delta}_s$.

Configuration for the range parameter δ_s	$D_0 = 5$		$D_0 = 10$		$D_0 = 15$		$D_0 = 20$		$D_0 = 25$	
	$\hat{\lambda}_s$	$\hat{\delta}_s$	$\hat{\lambda}_s$	$\hat{\delta}_s$	$\hat{\lambda}_s$	$\hat{\delta}_s$	$\hat{\lambda}_s$	$\hat{\delta}_s$	$\hat{\lambda}_s$	$\hat{\delta}_s$
Weakly non-stationary	1.16	0.02	0.44	0.01	0.25	0.00	0.18	0.00	0.15	0.00
Mildly non-stationary	1.33	0.03	0.61	0.01	0.44	0.01	0.34	0.01	0.3	0.01
Strongly non-stationary	1.38	0.03	0.69	0.01	0.55	0.02	0.47	0.02	0.45	0.02

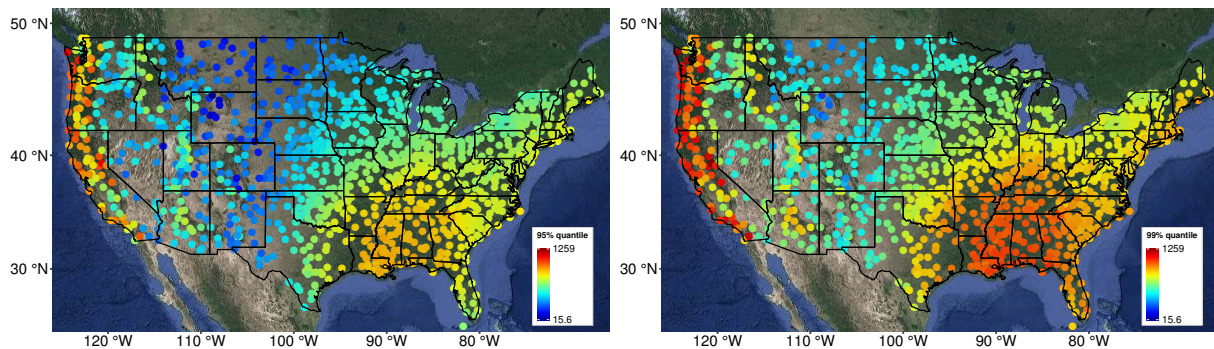


Figure 6: Empirical 95% (left) and 99% (right) quantiles of 5 day-cumulative winter precipitation data, observed at each of the monitoring stations, plotted on the same logarithmic color scale.

collected from 1900 to 2014 at the 1218 stations represented in Figure 1. To ensure data quality, we discard all observations marked by any reliability or accuracy flag. We focus on winter data (December 21 to March 20) to remove seasonal effects, and we consider 5 day-cumulative precipitation, in order to capture the intensity and duration of distinct storms, and to reduce the effect of temporal dependence. This procedure yields up to 2070 observations per station with 19.8% of missing data overall, which corresponds to about 2 million observations in total at all sites. The resulting dataset ranges from 0 (no rain over 5 days) to 3006 hundredths of an inch. The empirical 95% and 99% quantiles, plotted in Figure 6 using a logarithmic scale, reveal interesting spatial patterns that are due to both marginal distributions varying smoothly over space, and non-trivial spatial dependence that remains at high precipitation levels between close-by sites. In order to disentangle the local marginal and dependence effects, we use the two-step local censored likelihood estimation

approach described in Section 3 and fit the exponential factor copula model; recall Section 2.

5.2 Estimation grid and neighborhood selection

To describe the local dependence structure of precipitation extremes over the U.S., we generate a regular grid $\mathcal{G} \subset \mathcal{S}$ (using the WGS84/UTM zone 14N metric coordinate system) with 2200 grid points at an internodal distance of 60km. When plotted with respect to longitude and latitude, this results in a “distorted” grid, owing to the metric-to-degree system change.

An important step to fit our model for extremal dependence at each grid point $\mathbf{s}_0 \in \mathcal{G}$ using the local estimation approach described in Section 3 is to select a suitable number of nearest neighbors D_0 , which might vary over space. Although cross-validation techniques are usually advisable, pragmatic approaches are often adopted in practice: in the time series context, Davison and Ramesh (2000) suggest selecting the local likelihood bandwidth by the naked eye, while in the spatial context, Anderes and Stein (2011) advocate a heuristic method based on a measure of spatial variation in the estimated parameters. In principle, the choice of D_0 should be such that the spatial dependence structure of threshold exceedances is approximately stationary within each selected neighborhood $\mathcal{N}_{\mathbf{s}_0;D_0}$ around $\mathbf{s}_0 \in \mathcal{G}$. Small neighborhoods (with small D_0) yield good stationary approximations but poor statistical efficiency, and vice versa, and our simulation study in Section 4 suggests that D_0 should be as large as our computational resources permit, provided the dependence structure is not overly non-stationary. In the hydrological literature, a variety of tests to assess homogeneity of marginal distributions have been proposed; see for instance Lu and Stedinger (1992), Fill and Stedinger (1995), Hosking and Wallis (1993), and Hosking and Wallis (2005). Testing for stationarity of the extremal dependence structure is, however, much more complicated. Here, for simplicity, we assume that the local dependence structure of extremes is stationary whenever it is the case for margins, and we follow the recommendations of Viglione *et al.*

(2007) by testing homogeneity of the margins through a compromise between the Hosking and Wallis (1993) test and a modified Anderson–Darling test (Scholz and Stephens, 1987). Our ad-hoc neighborhood selection procedure can therefore be summarized as follows: considering an increasing nested sequence of neighborhoods, we test for marginal homogeneity until the test rejects the null hypothesis or a predefined maximum neighborhood size has been reached. In our case, we fix the maximum neighborhood to have radius 150km and, for computational reasons, $D_0 \leq 30$. Although this procedure has no theoretical guarantee to be optimal, we have found that it yields reasonable estimates with our dataset.

5.3 Local likelihood inference for extreme precipitation

Following Section 3, we fit the stationary exponential factor copula model (2.2) within small local neighborhoods, by maximizing the censored local log-likelihood (3.1) at all 2200 grid points $\mathbf{s}_0 \in \mathcal{G}$, choosing the empirical 95% quantile as threshold to define extreme events. The left-hand panel of Figure 6 illustrates the selected threshold at each monitoring station on the scale of the observations. As the smoothness parameter ν in (2.8) is difficult to estimate, we adopt a profile likelihood approach by considering a grid of values for ν . Among all grid points, the likelihood is maximized in 46.9%, 17.7%, 12.8%, 11.9% and 10.7% cases for $\nu = 0.5, 1, 1.5, 2, 2.5$, respectively. To be able to easily compare rate and scale parameter estimates across space, we then choose to fix $\nu = 0.5$ at all locations, which boils down to using an exponential correlation function for the underlying Gaussian process. Thanks to the embarrassingly parallel nature of our local likelihood estimation procedure, we can make an efficient use of distributed computing resources by fitting the local model at each grid point independently; overall, a single model fit (fixing $\nu = 0.5$, but estimating δ and λ) at all locations took about 25 thousands core-hours on a cluster with 39 nodes of 20 cores each.

Figure 7 shows the estimated log-rate $\log \lambda_{\mathbf{s}}$ and log-range $\log \delta_{\mathbf{s}}$ parameters, and their

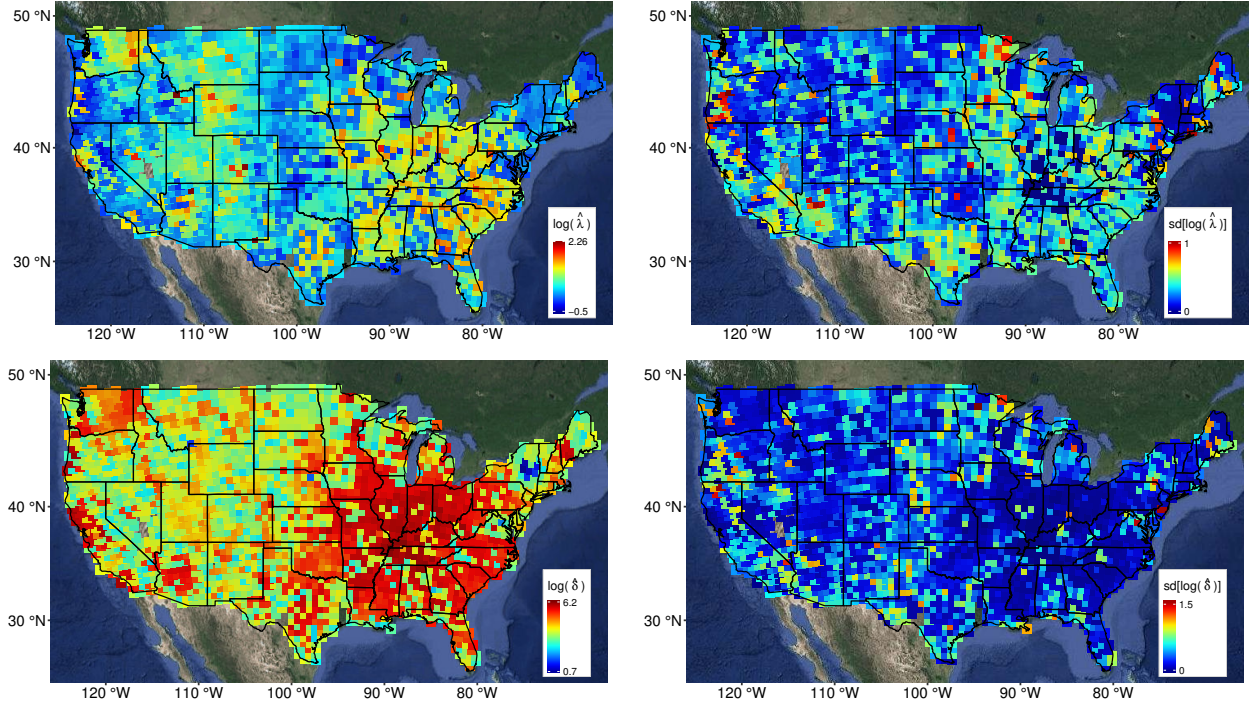


Figure 7: Estimated log-rate $\log \lambda_s$ (top left) and log-range $\log \delta_s$ (bottom left) parameters, with their standard deviations (right) computed from 300 block bootstrap samples with monthly blocks, for the model (2.7) fitted to the data described in Section 5.1.

estimated standard deviations computed over 300 block bootstrap samples with monthly blocks. Diverse spatial tail dependence structures arise in different regions, although the associated uncertainty appears quite high in some areas. To better understand and interpret the dynamics of the extremal dependence strength over space, Figure 8 displays the estimated local bivariate extremal coefficient, recall (2.9), at distance $h = 5, 20, 50, 100$ km. As expected, tail dependence weakens at larger distances, and the patterns are quite smoothly varying over space. Extremal dependence is stronger in the Pacific West, central region (except for Colorado), mid-South, mid-West and North East. By contrast, some states in the South East (e.g., North/South Carolina and Florida) and the Rocky Mountains show less extremal dependence, suggesting that extreme precipitation events are more localized in these regions.

To further validate our fitted model, Figure 2 compares empirical and fitted conditional tail probabilities, as defined in (1.1), clearly suggesting that our model succeeds in capturing

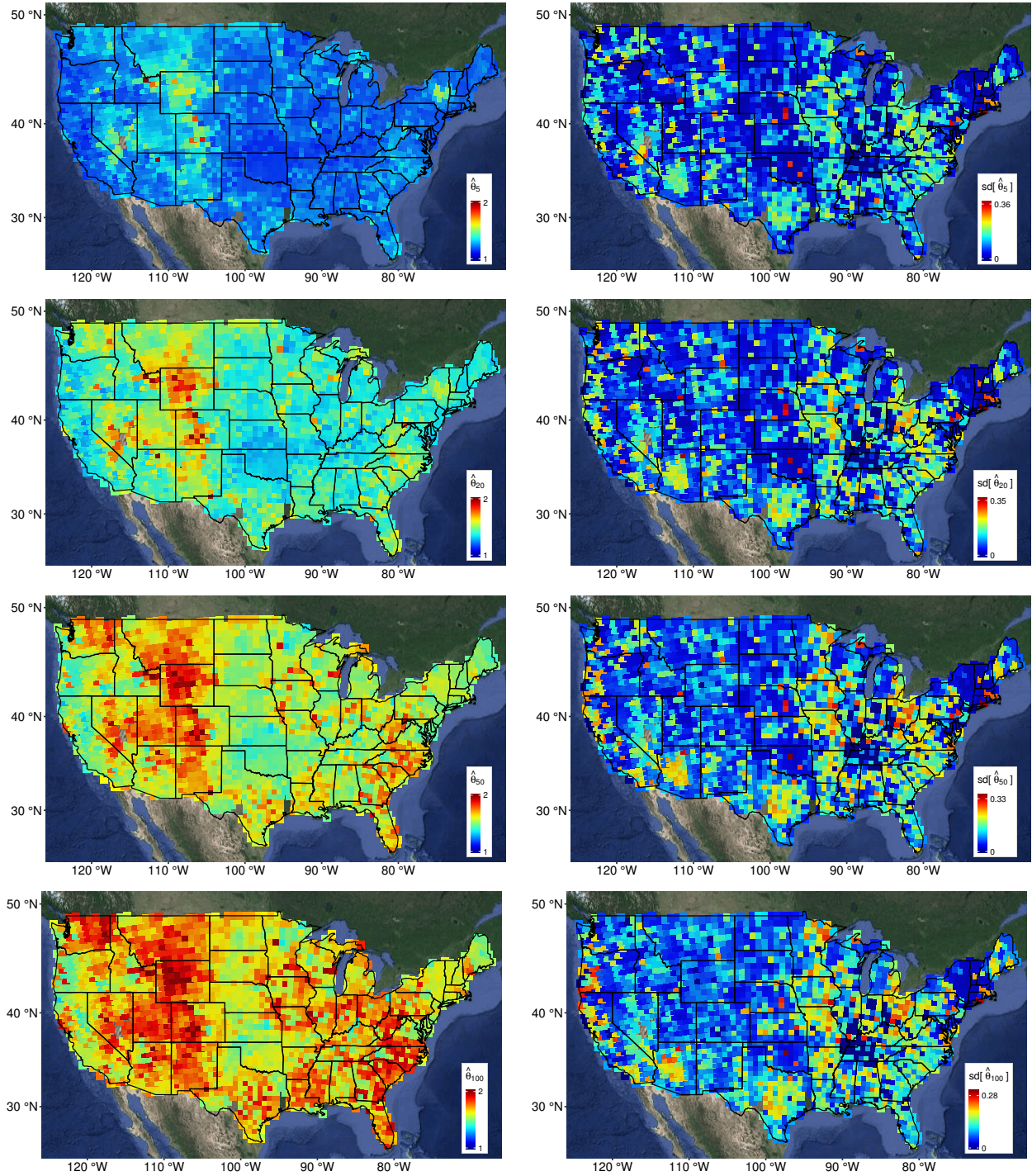


Figure 8: *Left*: Estimates of the local bivariate extremal coefficient at distance $h = 5, 20, 50, 100$ km (top to bottom). *Right*: Associated standard deviations.

weakening extremal dependence for close-by sites. Overall, our model has great tail flexibility, and our local estimation approach is able to uncover complex non-stationary patterns of

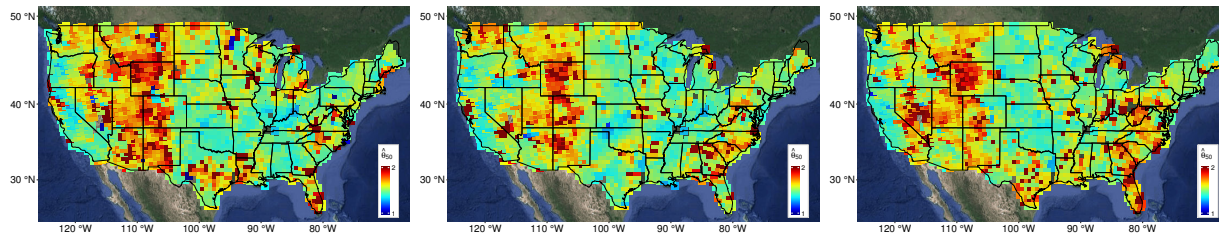


Figure 9: Estimates of the local bivariate extremal coefficient at $h = 50\text{km}$ for the subperiods 1920–1949 (left), 1950–1979 (middle) and 1980–2014 (right).

extremal dependence over space, which has important implications in terms of regional risk assessment of extreme precipitation events.

5.4 Subperiod analysis

We conclude our analysis of U.S. winter precipitation extremes, by analyzing whether or not their dependence structure has been stable through time. We fit our copula model again to the data in three distinct subperiods, chosen as 1920–1949, 1950–1979 and 1980–2014 in accordance with the overall trend observed in the global temperature anomalies (IPCC, 2014). Figure 9 reports the fitted local bivariate extremal coefficients at distance $h = 50\text{km}$. Although the spatial patterns are quite stable through time overall, and are fairly noisy owing to the smaller dataset used for each subperiod, the extremal dependence strength seems to have slightly increased in the North-West and South-East, suggesting that extreme precipitation events in these regions might be larger in extent nowadays than they were at the beginning of the past century. However, a small change in the joint tail dependence structure might result in an important difference in the return period of spatial extremes. To assess this, we compute, for each subperiod, the joint probability $p = \Pr\{Y_1 > F_1^{-1}(u), Y_2 > F_2^{-1}(u), Y_3 > F_3^{-1}(u)\}$, where $u = 0.95$, $Y_j = Y(\mathbf{s}_j) \sim F_j$ denote 5-day cumulative winter precipitation data, and \mathbf{s}_j , $j = 1, 2, 3$, are three fixed locations chosen in various states. The corresponding return period (in years), calculated as $1/(p \times N)$, where N is the number of 5-day periods in a year, is reported in Table 3 for Louisiana, Mississippi, Kentucky, Florida

Table 3: Return periods (in years) associated with the joint probability of observing an extreme precipitation event exceeding the 95% quantile at three locations simultaneously. The 1st column reports the state of these locations, while the 2nd column represents the thresholds (in hundredth of an inch) at each of the three selected locations. For comparison, these thresholds are roughly similar to the total rainfall measured in these states during the Katrina hurricane in August, 2005.

State	Thresholds	Return period (year)		
		1920–1949	1950–1979	1980–2014
Louisiana	{5.9, 7.3, 6.5}	10.3	7.7	1.6
Mississippi	{5.2, 4.7, 4.8}	23.1	7.8	1.8
Kentucky	{6.4, 7.5, 8.7}	14.8	14.2	6.3
Florida	{5.5, 10.9, 5.5}	34.4	12.8	1.2
Tennessee	{9.1, 6.9, 7.8}	19	17.2	15.5

and Tennessee, notorious to have experienced several extreme precipitation events in the recent past. Although these results may depend on the partition of the sample period and the selected locations, our findings strongly suggest that for these states, joint extreme precipitation events have become more frequent in recent years, which is in line with related studies (see, e.g., Wang *et al.*, 2017). We note, however, that the numbers reported in Table 3 need to be interpreted with care in view of the large stochastic, estimation and model uncertainties. More affirmative conclusions might be drawn from a deeper analysis.

6 Concluding remarks

To model sub-asymptotic spatial extremes over large heterogenous regions, we propose a flexible non-stationary factor copula model, fitted locally, that can capture weakening dependence strength as events become more extreme. This contrasts with the current spatial extremes literature, which often relies on asymptotic models with a rigid tail structure. Our model can be efficiently fitted to high threshold exceedances using a local censored likelihood estimation procedure at a reasonable computational burden. Our extensive simulation experiments demonstrate the flexibility of our model and the efficiency of our local estimation approach, while providing some guidance on the selection of regional neighborhoods.

By fitting the model to precipitation data over the whole contiguous U.S., a diverse and

complex tail dependence structure emerges, revealing rich and intuitive spatial patterns. Further analysis on distinct subperiods suggests that in certain states, spatial extreme precipitation events have become more frequent in recent years.

Although our proposed non-stationary model has great additional flexibility over its stationary counterpart, it is still unable to capture weak dependence at large distances, which is, however, a common feature of most models for spatial extremes. This implies that the fitted model needs to be interpreted locally, or perhaps regionally. Further research should therefore be devoted in developing models for spatial and spatio-temporal extremes that can more realistically capture long-range independence.

Acknowledgements

We thank Luigi Lombardo (KAUST) for cartographic support and Eduardo González (KAUST) for computational support. We extend our thanks to Dan Cooley (Colorado State University) for helpful comments and suggestions. Support from the KAUST Supercomputing Laboratory and access to Shaheen is also gratefully acknowledged.

A Simplified expressions for the model likelihood

In this appendix, we obtain simplified expressions for the local censored likelihood function (3.1) based on Model (2.2) (and stemming from (2.7)), in order to compute the maximum likelihood estimates in a reasonable time, while avoiding numerical instabilities.

A.1 Joint density of the W process in (2.2)

From expression (2.4), one has

$$\begin{aligned} f_D^{\mathbf{w}}(\mathbf{w}) &= \lambda \int_0^\infty \phi_D(\mathbf{w} - v\mathbf{1}_D; \boldsymbol{\Sigma}_{\mathbf{z}}) \exp(-\lambda v) dv \\ &= \lambda \int_0^\infty (2\pi)^{-D/2} (\det \boldsymbol{\Sigma}_{\mathbf{z}})^{-1/2} \exp\left(\frac{a_4^2 a_3 - a_1}{2}\right) \exp\left\{-\frac{1}{2a_3^{-1}}(v - a_4)^2\right\} dv \end{aligned}$$

$$= \lambda(2\pi)^{-(D-1)/2} a_3^{-1/2} (\det \boldsymbol{\Sigma}_{\mathbf{Z}})^{-1/2} \exp\left(\frac{a_4^2 a_3 - a_1}{2}\right) \Phi(a_3^{1/2} a_4),$$

where $a_1 = \mathbf{w}^T \boldsymbol{\Sigma}_{\mathbf{Z}}^{-1} \mathbf{w}$, $a_2 = \mathbf{1}_D^T \boldsymbol{\Sigma}_{\mathbf{Z}}^{-1} \mathbf{w}$, $a_3 = \mathbf{1}_D^T \boldsymbol{\Sigma}_{\mathbf{Z}}^{-1} \mathbf{1}_D$, $a_4 = (a_2 - \lambda)/a_3$, $\mathbf{w} = (w_1, \dots, w_D)^T$, $\mathbf{1}_D = (1, \dots, 1)^T \in \mathbb{R}^D$. The marginal density $f_1^{\mathbf{W}}(w; \lambda)$ with $D = 1$ can be easily deduced.

A.2 Joint distribution of the W process in (2.2)

Here we express the finite-dimensional distribution $F_D^{\mathbf{W}}$ as a function of conditional multivariate normal distributions. This alternative formulation allows us to use efficient routines implemented in R, substantially improving accuracy and execution time. Using integration by parts in expression (2.3), one obtains

$$\begin{aligned} F_D^{\mathbf{W}}(\mathbf{w}) &= \Phi_D(\mathbf{w}; \boldsymbol{\Sigma}_{\mathbf{Z}}) - \sum_{j=1}^D \int_0^\infty \Phi_{D-1}(\mathbf{w}_{-j} - v \mathbf{1}_{D-1} - \mu_{|j}; \boldsymbol{\Sigma}_{\mathbf{Z}|j}) \phi(w_j - v) \exp(-\lambda v) dv \\ &= \Phi_D(\mathbf{w}; \boldsymbol{\Sigma}_{\mathbf{Z}}) - \sum_{j=1}^D \exp\left(\frac{\lambda^2}{2} - \lambda w_j\right) \int_0^\infty \Phi_{D-1}(\mathbf{w}_{-j} - v \mathbf{1}_{D-1} - \mu_{|j}; \boldsymbol{\Sigma}_{\mathbf{Z}|j}) \phi(v - w_j + \lambda) dv, \end{aligned}$$

where $\mathbf{w}_{-j} = (w_1, \dots, w_{j-1}, w_{j+1}, \dots, w_D)^T \in \mathbb{R}^{D-1}$ and $\mu_{|j}$ and $\boldsymbol{\Sigma}_{\mathbf{Z}|j}$ are the conditional mean and covariance matrix of $\mathbf{w}_{-j}|w_j$, respectively. Precisely,

$$\mu_{|j} = \boldsymbol{\Sigma}_{\mathbf{z};-j,j}(w_j - v), \quad \boldsymbol{\Sigma}_{\mathbf{Z}|j} = \boldsymbol{\Sigma}_{\mathbf{z};-j,-j} - \boldsymbol{\Sigma}_{\mathbf{z};-j,j} \boldsymbol{\Sigma}_{\mathbf{z};-j,j}^T, \quad j = 1, \dots, D,$$

where $\boldsymbol{\Sigma}_{\mathbf{z};-j,j}$ denotes the j th column of the matrix $\boldsymbol{\Sigma}_{\mathbf{Z}}$ with the j th row removed, etc. Now,

$$\begin{aligned} &\int_0^\infty \Phi_{D-1}(\mathbf{w}_{-j} - v \mathbf{1}_{D-1} - \mu_{|j}; \boldsymbol{\Sigma}_{\mathbf{Z}|j}) \phi(v - w_j + \lambda) dv \\ &= \int_0^\infty \Phi_{D-1}\{\mathbf{w}_{-j} - \boldsymbol{\Sigma}_{\mathbf{z};-j,j} w_j - v(\mathbf{1}_{D-1} - \boldsymbol{\Sigma}_{\mathbf{z};-j,j}); \boldsymbol{\Sigma}_{\mathbf{Z}|j}\} \phi(v - w_j + \lambda) dv \\ &= \Pr\left(\mathbf{Y} \leq \boldsymbol{\Sigma}_{\mathbf{Z}|j}^{-1/2} \left\{ \mathbf{w}_{-j} - \boldsymbol{\Sigma}_{\mathbf{z};-j,j} w_j - \tilde{V}(\mathbf{1}_{D-1} - \boldsymbol{\Sigma}_{\mathbf{z};-j,j}) \right\}, \tilde{V} > 0\right) \\ &= \Pr\left(\mathbf{Q}_j \leq \mathbf{w}_{-j} - \boldsymbol{\Sigma}_{\mathbf{z};-j,j} w_j, -\tilde{V} \leq 0\right) \end{aligned} \tag{A.1}$$

where $\mathbf{Y} \sim \mathcal{N}(\mathbf{0}, \mathbf{I}_{D-1})$ follows the standard multivariate normal distribution in dimension $D-1$, and is independent of the univariate normal random variable \tilde{V} with mean $w_j - \lambda$ and

unit variance, and where $\mathbf{Q}_j = \Sigma_{\mathbf{Z}|j}^{1/2} \mathbf{Y} + \tilde{V}(\mathbf{1}_{D-1} - \Sigma_{\mathbf{Z};-j,j})$. To compute (A.1), notice that the D -dimensional vector $\mathbf{Q}_{j,0} = (\mathbf{Q}_j^T, -\tilde{V})^T$ is jointly multivariate normal, and that \mathbf{Q}_j has mean $(w_j - \lambda)(\mathbf{1}_{D-1} - \Sigma_{\mathbf{Z};-j,j})$ and covariance matrix $\Sigma_{\mathbf{Z}|j} + (\mathbf{1}_{D-1} - \Sigma_{\mathbf{Z};-j,j})(\mathbf{1}_{D-1} - \Sigma_{\mathbf{Z};-j,j})^T = \mathbf{1}_{D-1} \mathbf{1}_{D-1}^T - 2\mathbf{1}_{D-1} \Sigma_{\mathbf{Z};-j,j}^T + \Sigma_{\mathbf{Z};-j,-j}$. Hence, one has

$$\Pr\left(\mathbf{Q}_j \leq \mathbf{w}_{-j} - \Sigma_{\mathbf{Z};-j,j} w_j, -\tilde{V} \leq 0\right) = \Pr\left(\mathbf{Q}_{j,0} \leq \mathbf{q}_{j,0}\right), \quad \mathbf{Q}_{j,0} = (\mathbf{Q}_j^T, -\tilde{V})^T \sim \mathcal{N}_D(\mu_{j,0}, \mathbf{\Omega}_{j,0}),$$

where

$$\begin{aligned} \mathbf{q}_{j,0} &= \begin{pmatrix} \mathbf{w}_{-j} - \Sigma_{\mathbf{Z};-j,j} w_j \\ 0 \end{pmatrix}, \quad \mu_{j,0} = \begin{pmatrix} (w_j - \lambda)(\mathbf{1}_{D-1} - \Sigma_{\mathbf{Z};-j,j}) \\ \lambda - w_j \end{pmatrix}, \\ \mathbf{\Omega}_{j,0} &= \begin{pmatrix} \mathbf{1}_{D-1} \mathbf{1}_{D-1}^T - 2\Sigma_{\mathbf{Z};-j,j} + \Sigma_{\mathbf{Z};-j,-j} & \Sigma_{\mathbf{Z};-j,j} - \mathbf{1}_{D-1} \\ \Sigma_{\mathbf{Z};-j,j} - \mathbf{1}_{D-1} & 1 \end{pmatrix}. \end{aligned}$$

Finally, one obtains

$$F_D^{\mathbf{W}}(\mathbf{w}) = \Phi_D(\mathbf{w}; \Sigma_{\mathbf{Z}}) - \sum_{j=1}^D \exp\left(\frac{\lambda^2}{2} - \lambda w_j\right) \Phi_D(\mathbf{q}_{j,0} - \mu_{j,0}; \mathbf{\Omega}_{j,0}). \quad (\text{A.2})$$

In particular, by setting $D = 1$, the marginal distribution may be written as

$$F_1^{\mathbf{W}}(w; \lambda) = \Phi(w) - \exp(\lambda^2/2 - \lambda w) \Phi(w - \lambda). \quad (\text{A.3})$$

A.3 Partial derivatives of the joint distribution $F_D^{\mathbf{W}}$

We want to compute $\partial_{J_i} F_D^{\mathbf{W}}$, the partial derivative of $F_D^{\mathbf{W}}$ with respect to the variables indexed by the set $J_i \subseteq \{1, \dots, D\}$. Without loss of generality, we here assume that $J_i = \{1, \dots, k\}$, for some integer $1 \leq k \leq D-1$. Writing $r = D-k$, one can express the covariance matrix $\Sigma_{\mathbf{Z}}$ in block notation as follows:

$$\Sigma_{\mathbf{Z}} = \begin{pmatrix} \Sigma_{\mathbf{Z},k} & \Sigma_{\mathbf{Z},rk}^T \\ \Sigma_{\mathbf{Z},rk} & \Sigma_{\mathbf{Z},r} \end{pmatrix}.$$

Then, writing $\mathbf{w} = (\mathbf{w}_k^T, \mathbf{w}_r^T)^T$, with $\mathbf{w}_k = (w_1, \dots, w_k)^T$ and $\mathbf{w}_r = (w_{k+1}, \dots, w_D)^T$, one has

$$\partial_{J_i} F_D^{\mathbf{W}}(\mathbf{w}) = \partial_{1:k}^k \lambda \int_0^\infty \Phi_D(\mathbf{w} - v \mathbf{1}_D; \Sigma_{\mathbf{Z}}) \exp(-\lambda v) dv$$

$$= \lambda \int_0^\infty \phi_k(\mathbf{w}_k - v\mathbf{1}_k; \Sigma_{\mathbf{Z},k}) \Phi_r(\mathbf{w}_r - v\mathbf{1}_r - \mu_{|k}; \Sigma_{\mathbf{Z}|k}) \exp(-\lambda v) dv,$$

where $\mu_{|k}$ and $\Sigma_{\mathbf{Z}|k}$ are the conditional mean and covariance of $\mathbf{w}_r \mid \mathbf{w}_k$, respectively, and are obtained as

$$\mu_{|k} = \Sigma_{\mathbf{Z},rk} \Sigma_{\mathbf{Z},k}^{-1} (\mathbf{w}_k - v\mathbf{1}_k), \quad \Sigma_{\mathbf{Z}|k} = \Sigma_{\mathbf{Z},r} - \Sigma_{\mathbf{Z},rk} \Sigma_{\mathbf{Z},k}^{-1} \Sigma_{\mathbf{Z},rk}^T.$$

Tedious but straightforward calculations yield $\phi_k(\mathbf{w}_k - v\mathbf{1}_k; \Sigma_{\mathbf{Z},k}) \exp(-\lambda v) = C \phi\{b_3^{1/2}(v - b_4)\}$, where $C = (2\pi)^{-(k-1)/2} b_3^{-1/2} (\det \Sigma_{\mathbf{Z},k})^{-1/2} \exp\{(b_4^2 b_3 - b_1)/2\}$, with $b_1 = \mathbf{w}_k^T \Sigma_{\mathbf{Z},k}^{-1} \mathbf{w}_k$, $b_2 = \mathbf{1}_k^T \Sigma_{\mathbf{Z},k}^{-1} \mathbf{w}_k$, $b_3 = \mathbf{1}_k^T \Sigma_{\mathbf{Z},k}^{-1} \mathbf{1}_k$, and $b_4 = (b_2 - \lambda)/b_3$. Therefore,

$$\begin{aligned} \partial_{J_i} F_D^{\mathbf{W}}(\mathbf{w}) &= \lambda C \int_0^\infty \phi\{b_3^{1/2}(v - b_4)\} \Phi_r(\mathbf{w}_r - v\mathbf{1}_r - \mu_{|k}; \Sigma_{\mathbf{Z}|k}) dv \\ &= \lambda C \int_0^\infty \phi\{b_3^{1/2}(v - b_4)\} \Phi_r\{\mathbf{w}_r - \Sigma_{\mathbf{Z},rk} \Sigma_{\mathbf{Z},k}^{-1} \mathbf{w}_k - v(\mathbf{1}_r - \Sigma_{\mathbf{Z},rk} \Sigma_{\mathbf{Z},k}^{-1} \mathbf{1}_k); \Sigma_{\mathbf{Z}|k}\} dv \\ &= \lambda C \Pr\left(\mathbf{Y} \leq \Sigma_{\mathbf{Z}|k}^{-1/2} \left\{ \mathbf{w}_r - \Sigma_{\mathbf{Z},rk} \Sigma_{\mathbf{Z},k}^{-1} \mathbf{w}_k - \tilde{V}(\mathbf{1}_r - \Sigma_{\mathbf{Z},rk} \Sigma_{\mathbf{Z},k}^{-1} \mathbf{1}_k) \right\}, \tilde{V} > 0\right) \\ &= \lambda C \Pr\left(\mathbf{Q}_r \leq \mathbf{w}_r - \Sigma_{\mathbf{Z},rk} \Sigma_{\mathbf{Z},k}^{-1} \mathbf{w}_k, -\tilde{V} \leq 0\right), \end{aligned} \quad (\text{A.4})$$

where $\mathbf{Y} \sim \mathcal{N}(\mathbf{0}, \mathbf{I}_r)$ has the standard multivariate normal distribution in dimension r , and is independent of the univariate normal random variable \tilde{V} with mean b_4 and variance b_3^{-1} , and where $\mathbf{Q}_r = \Sigma_{\mathbf{Z}|k}^{1/2} \mathbf{Y} + \tilde{V}(\mathbf{1}_r - \Sigma_{\mathbf{Z},rk} \Sigma_{\mathbf{Z},k}^{-1} \mathbf{1}_k)$. To compute (A.4), notice that the $(r+1)$ -dimensional vector $\mathbf{Q}_{r,0} = (\mathbf{Q}_r^T, -\tilde{V})^T$ is jointly multivariate normal, and that \mathbf{Q}_r has mean $b_4(\mathbf{1}_r - \Sigma_{\mathbf{Z},rk} \Sigma_{\mathbf{Z},k}^{-1} \mathbf{1}_k)$ and covariance $\Sigma_{\mathbf{Z}|k} + b_3^{-1}(\mathbf{1}_r - \Sigma_{\mathbf{Z},rk} \Sigma_{\mathbf{Z},k}^{-1} \mathbf{1}_k)(\mathbf{1}_r - \Sigma_{\mathbf{Z},rk} \Sigma_{\mathbf{Z},k}^{-1} \mathbf{1}_k)^T$. Hence,

$$\Pr\left(\mathbf{Q}_r \leq \mathbf{w}_r - \Sigma_{\mathbf{Z},rk} \Sigma_{\mathbf{Z},k}^{-1} \mathbf{w}_k, -\tilde{V} \leq 0\right) = \Pr(\mathbf{Q}_{r,0} \leq \mathbf{q}_{r,0}),$$

where $\mathbf{Q}_{r,0} = (\mathbf{Q}_r^T, -\tilde{V})^T \sim \mathcal{N}_{r+1}(\mu_{r,0}, \Omega_{r,0})$ and

$$\begin{aligned} \mathbf{q}_{r,0} &= \begin{pmatrix} \mathbf{w}_r - \Sigma_{\mathbf{Z},rk} \Sigma_{\mathbf{Z},k}^{-1} \mathbf{w}_k \\ 0 \end{pmatrix}, \quad \mu_{r,0} = \begin{pmatrix} b_4(\mathbf{1}_r - \Sigma_{\mathbf{Z},rk} \Sigma_{\mathbf{Z},k}^{-1} \mathbf{1}_k) \\ -b_4 \end{pmatrix}, \\ \Omega_{r,0} &= \begin{pmatrix} \Sigma_{\mathbf{Z}|k} + b_3^{-1}(\mathbf{1}_r - \Sigma_{\mathbf{Z},rk} \Sigma_{\mathbf{Z},k}^{-1} \mathbf{1}_k)(\mathbf{1}_r - \Sigma_{\mathbf{Z},rk} \Sigma_{\mathbf{Z},k}^{-1} \mathbf{1}_k)^T & b_3^{-1}(\Sigma_{\mathbf{Z},rk} \Sigma_{\mathbf{Z},k}^{-1} \mathbf{1}_k - \mathbf{1}_r) \\ b_3^{-1}(\Sigma_{\mathbf{Z},rk} \Sigma_{\mathbf{Z},k}^{-1} \mathbf{1}_k - \mathbf{1}_r)^T & b_3^{-1} \end{pmatrix}. \end{aligned}$$

Finally, one obtains

$$\partial_{J_i} F_D^{\mathbf{W}}(\mathbf{w}) = \lambda C \Phi_{r+1}(\mathbf{q}_{r,0} - \mu_{r,0}; \Omega_{r,0}).$$

B Tail properties of the non-stationary exponential factor copula model

In this appendix, we provide detailed information on the sub-asymptotic joint tail behavior of the stationary exponential factor model (2.2), and we study the limiting extremal dependence structure of the non-stationary model (2.7).

Lemma 1. *In Model (2.7), the marginal distribution at site $\mathbf{s} \in \mathcal{S}$, $F_{1;\mathbf{s}}^{\mathbf{W}}(w; \lambda_{\mathbf{s}})$, satisfies*

$$F_{1;\mathbf{s}}^{\mathbf{W}}(w; \lambda_{\mathbf{s}}) = 1 - \exp(\lambda_{\mathbf{s}}^2/2 - \lambda_{\mathbf{s}}w) + \lambda_{\mathbf{s}}\phi(w)\{w(w - \lambda_{\mathbf{s}})\}^{-1} + O\{\phi(w)w^{-4}\}, \quad w \rightarrow \infty.$$

Proof. From (A.3), one has $F_{1;\mathbf{s}}^{\mathbf{W}}(w; \lambda_{\mathbf{s}}) = \Phi(w) - \Phi(w - \lambda_{\mathbf{s}})\exp(\lambda_{\mathbf{s}}^2/2 - \lambda_{\mathbf{s}}w)$. Furthermore, thanks to a well-known expansion of the Gaussian tail, one has

$$1 - \Phi(w) = \phi(w)\{w^{-1} - w^{-3} + O(w^{-5})\}, \quad w \rightarrow \infty. \quad (\text{B.1})$$

Plugging (B.1) into the expression for $F_{1;\mathbf{s}}^{\mathbf{W}}(w; \lambda_{\mathbf{s}})$ yields, as $w \rightarrow \infty$,

$$\begin{aligned} F_{1;\mathbf{s}}^{\mathbf{W}}(w; \lambda_{\mathbf{s}}) &= 1 - \phi(w)\{w^{-1} - w^{-3} + O(w^{-5})\} \\ &\quad - [1 - \phi(w - \lambda_{\mathbf{s}})\{(w - \lambda_{\mathbf{s}})^{-1} - (w - \lambda_{\mathbf{s}})^{-3} + O(w^{-5})\}] \exp(\lambda_{\mathbf{s}}^2/2 - \lambda_{\mathbf{s}}w) \\ &= 1 - \exp(\lambda_{\mathbf{s}}^2/2 - \lambda_{\mathbf{s}}w) + \phi(w) [(w - \lambda_{\mathbf{s}})^{-1} - (w - \lambda_{\mathbf{s}})^{-3} - w^{-1} + w^{-3} + O(w^{-5})] \\ &= 1 - \exp(\lambda_{\mathbf{s}}^2/2 - \lambda_{\mathbf{s}}w) + \lambda_{\mathbf{s}}\phi(w)\{w(w - \lambda_{\mathbf{s}})\}^{-1} + O\{\phi(w)w^{-4}\}. \end{aligned}$$

□

Lemma 2. *In Model (2.7), the marginal quantile function at location $\mathbf{s} \in \mathcal{S}$, $q_{\mathbf{s}}^{\mathbf{W}}(t; \lambda_{\mathbf{s}}) = F_{1;\mathbf{s}}^{\mathbf{W}-1}(1 - t^{-1}; \lambda_{\mathbf{s}})$, admits the expansion*

$$q_{\mathbf{s}}^{\mathbf{W}}(t; \lambda_{\mathbf{s}}) = \lambda_{\mathbf{s}}^{-1} \log t + \lambda_{\mathbf{s}}/2 - t \frac{\phi(\lambda_{\mathbf{s}}^{-1} \log t + \lambda_{\mathbf{s}}/2)}{\lambda_{\mathbf{s}}^{-2} \log^2 t - \lambda_{\mathbf{s}}^2/4} \{1 + o(1)\}, \quad t \rightarrow \infty.$$

Proof. From notational convenience, we shall write $q(t) \equiv q_{\mathbf{s}}^{\mathbf{W}}(t; \lambda_{\mathbf{s}})$. Because $1 - F_{1;\mathbf{s}}^{\mathbf{W}}\{q(t)\} = t^{-1}$ and $q(t) \rightarrow \infty$ as $t \rightarrow \infty$, one has from Lemma 1 that

$$\exp\{\lambda_{\mathbf{s}}^2/2 - \lambda_{\mathbf{s}}q(t)\} - \lambda_{\mathbf{s}}\phi\{q(t)\} [q(t)\{q(t) - \lambda_{\mathbf{s}}\}]^{-1} + O[\phi\{q(t)\}q(t)^{-4}] = t^{-1}. \quad (\text{B.2})$$

Noting that the leftmost term in (B.2) is dominant, this yields

$$q(t) = \lambda_s^{-1} \log t + \lambda_s/2 + r(t), \quad (\text{B.3})$$

where $r(t) \rightarrow 0$, as $t \rightarrow \infty$. Using (B.3) back into (B.2) gives

$$t^{-1} \exp\{-\lambda_s r(t)\} - \lambda_s \frac{\phi(\lambda_s^{-1} \log t + \lambda_s/2)}{\lambda_s^{-2} \log^2 t - \lambda_s^2/4} \{1 + o(1)\} = t^{-1}.$$

Thus, because $\exp(-x) = 1 - x\{1 + o(1)\}$, as $x \rightarrow 0$, one obtains

$$r(t) = -t \frac{\phi(\lambda_s^{-1} \log t + \lambda_s/2)}{\lambda_s^{-2} \log^2 t - \lambda_s^2/4} \{1 + o(1)\},$$

which, combined with (B.3), concludes the proof. \square

Proof of Proposition 1. Consider the stationary exponential factor model (2.2), and let

$z(u) = F_1^{\mathbf{W}^{-1}}(u; \lambda)$ denote univariate quantiles. Thanks to (A.2), one has

$$\begin{aligned} C_2^{\mathbf{W}}(u, u) &= F_2^{\mathbf{W}}\{z(u), z(u)\} \\ &= \Phi_2\{z(u), z(u); \Sigma_{\mathbf{Z}}\} - 2 \exp\{\lambda^2/2 - \lambda z(u)\} \Phi_2[\lambda\{1 - \rho(h)\}, z(u) - \lambda; \mathbf{\Omega}], \\ &= \Phi_2\{z(u), z(u); \Sigma_{\mathbf{Z}}\} - 2 \exp\{\lambda^2/2 - \lambda z(u)\} \Phi_2\left[\lambda\sqrt{\{1 - \rho(h)\}/2}, z(u) - \lambda; \tilde{\mathbf{\Omega}}\right], \end{aligned} \quad (\text{B.4})$$

where $\rho(h)$ is the underlying correlation function, and the covariance matrices $\mathbf{\Omega}$ and $\tilde{\mathbf{\Omega}}$ are

$$\mathbf{\Omega} = \begin{pmatrix} 2\{1 - \rho(h)\} & -\{1 - \rho(h)\} \\ -\{1 - \rho(h)\} & 1 \end{pmatrix}, \quad \tilde{\mathbf{\Omega}} = \begin{pmatrix} 1 & -\sqrt{\{1 - \rho(h)\}/2} \\ -\sqrt{\{1 - \rho(h)\}/2} & 1 \end{pmatrix}.$$

Now, thanks to Lemma 2, $z(u) = q_s^{\mathbf{W}}\{(1 - u)^{-1}; \lambda\} = -\lambda^{-1} \log(1 - u) + \lambda/2 + s(u)$, with

$$s(u) = -\frac{\phi\{z(u)\}}{(1 - u)z(u)\{z(u) - \lambda\}} \{1 + o(1)\}, \quad u \rightarrow 1, \quad (\text{B.5})$$

such that $s(u) \rightarrow 0$, $z(u) = -\lambda^{-1} \log(1 - u) + \lambda/2 \{1 + o(1)\}$, and $z(u) \rightarrow \infty$, as $u \rightarrow 1$.

Consequently, from the definition (1.1) and (B.4)–(B.5), one can write

$$\chi_h(u) = \frac{1 - 2u + C_2^{\mathbf{W}}(u, u)}{1 - u} = 2 - \frac{1 - C_2^{\mathbf{W}}(u, u)}{1 - u} = 2 - f(u) - g(u)h(u), \quad (\text{B.6})$$

where, using the bivariate Gaussian survivor function $\bar{\Phi}_2$, one has

$$\begin{aligned} f(u) &= \frac{1 - \Phi_2\{z(u), z(u); \Sigma_{\mathbf{Z}}\}}{1 - u} = \frac{2[1 - \Phi\{z(u)\}] - \bar{\Phi}_2\{z(u), z(u); \Sigma_{\mathbf{Z}}\}}{1 - u} \\ &= \frac{2[1 - \Phi\{z(u)\}]\{1 + o(1)\}}{1 - u} = \frac{2\phi\{z(u)\}}{(1 - u)z(u)}\{1 + o(1)\} \rightarrow 0, \quad u \rightarrow 1; \end{aligned} \quad (\text{B.7})$$

$$g(u) = \frac{\exp\{\lambda^2/2 - \lambda z(u)\}}{1 - u} = \exp\{-\lambda s(u)\} \rightarrow 1, \quad u \rightarrow 1; \quad (\text{B.8})$$

$$h(u) = 2\Phi_2\left[\lambda\sqrt{\{1 - \rho(h)\}/2}, z(u) - \lambda; \tilde{\Sigma}\right] \rightarrow 2\Phi\left[\lambda\sqrt{\{1 - \rho(h)\}/2}\right], \quad u \rightarrow 1. \quad (\text{B.9})$$

The 3rd equality in (B.7) is true as bivariate Gaussian random vectors $(Z_1, Z_2)^T$ with correlation $\rho < 1$ are tail-independent, i.e., $\Pr(Z_1 > z \mid Z_2 > z) \rightarrow 0$, as $z \rightarrow \infty$ (Ledford and Tawn, 1996); the expansion in the 4th equality in (B.7) is due to (B.1); finally, $f(u) \rightarrow 0$, as $\phi\{z(u)\}/(1 - u) \sim (2\pi)^{-1/2} \exp\{-\log^2(1 - u)/2 - \log(1 - u)\} \rightarrow 0$, as $u \rightarrow 1$.

Equations (B.6)–(B.9) imply that $\chi_h = \lim_{u \rightarrow 1} \chi_h(u) = 2 - 2\Phi[\lambda\sqrt{\{1 - \rho(h)\}/2}]$. Hence, by writing $A = \lambda\sqrt{\{1 - \rho(h)\}/2}$, one obtains as $u \rightarrow 1$

$$\begin{aligned} \chi_h(u) - \chi_h &= 2\Phi(A) - f(u) - g(u)h(u) \\ &= -f(u) + 2\Phi(A) \left[1 - \exp\{-\lambda s(u)\} \frac{\Phi_2\left\{A, z(u) - \lambda; \tilde{\Sigma}\right\}}{\Phi(A)} \right] \\ &= -f(u) + 2\Phi(A) [1 - \{1 - \lambda s(u)\}\{1 - k(u)\}\{1 + o(1)\}] \\ &= -f(u) + 2\Phi(A) \{\lambda s(u) + k(u)\} \{1 + o(1)\}, \end{aligned} \quad (\text{B.10})$$

where $k(u) = [\Phi(A) - \Phi_2\{A, z(u) - \lambda; \tilde{\Sigma}\}]/\Phi(A)$. Notice that by the l'Hospital's rule, it can be verified that for $\rho(h) > 0$, $k(u)$ satisfies

$$k(u) = \frac{1 - \Phi\{z(u) - \lambda\}}{\Phi(A)}\{1 + o(1)\} = \frac{\phi\{z(u) - \lambda\}}{\Phi(A)\{z(u) - \lambda\}}\{1 + o(1)\} \rightarrow 0, \quad u \rightarrow 1. \quad (\text{B.11})$$

Comparing the rates of convergence of $s(u)$, $f(u)$ and $k(u)$ in (B.5), (B.7) and (B.11), respectively, we deduce that $f(u)$ is dominant as $u \rightarrow 1$, and therefore from (B.10), one has

$$\chi_h(u) - \chi_h = -f(u)\{1 + o(1)\} = -\frac{2\phi\{z(u)\}}{(1 - u)z(u)}\{1 + o(1)\} = -\frac{2\phi\{-\lambda^{-1} \log(1 - u) + \lambda/2\}}{(1 - u)\{-\lambda^{-1} \log(1 - u) + \lambda/2\}}\{1 + o(1)\},$$

which concludes the proof. \square

Proof of Proposition 2. By Lemma 2, one has $F_{1;\mathbf{s}}^{\mathbf{W}^{-1}}(1 - qx; \lambda_{\mathbf{s}}) = q_{\mathbf{s}}^{\mathbf{W}}\{(qx)^{-1}; \lambda_{\mathbf{s}}\} = -\lambda_{\mathbf{s}}^{-1}(\log q + \log x) + \lambda_{\mathbf{s}}/2\{1 + o(1)\}$, as $q \rightarrow 0$, for any $x > 0$. Moreover, extending the proof of (A.2), one can show that for the non-stationary exponential factor copula model, one has

$$F_{2;\mathbf{s}_1, \mathbf{s}_2}^{\mathbf{W}}(w_1, w_2) = \Phi_2(w_1, w_2; \boldsymbol{\Sigma}_{\mathbf{Z}}) - \sum_{j=1}^2 \exp\left(\frac{\lambda_{\mathbf{s}_j}}{2} - \lambda_{\mathbf{s}_j} w_j\right) \Phi_2(\mathbf{q}_{j,0} - \mu_{j,0}; \boldsymbol{\Omega}_{j,0}),$$

where

$$\mathbf{q}_{1,0} = \begin{pmatrix} w_2 - \rho(h)w_1 \\ 0 \end{pmatrix}, \quad \mu_{1,0} = \begin{pmatrix} \{\lambda_{\mathbf{s}_2}^{-1} - \rho(h)\lambda_{\mathbf{s}_1}^{-1}\}\{\lambda_{\mathbf{s}_1}w_1 - \lambda_{\mathbf{s}_1}^2\} \\ \lambda_{\mathbf{s}_1}^2 - \lambda_{\mathbf{s}_1}w_1 \end{pmatrix},$$

$$\boldsymbol{\Omega}_{1,0} = \begin{pmatrix} 1 + \lambda_{\mathbf{s}_1}^2\lambda_{\mathbf{s}_2}^{-2} - 2\rho(h)\lambda_{\mathbf{s}_1}\lambda_{\mathbf{s}_2}^{-1} & \rho(h)\lambda_{\mathbf{s}_1} - \lambda_{\mathbf{s}_2}^{-1}\lambda_{\mathbf{s}_1}^2 \\ \rho(h)\lambda_{\mathbf{s}_1} - \lambda_{\mathbf{s}_2}^{-1}\lambda_{\mathbf{s}_1}^2 & \lambda_{\mathbf{s}_1}^2 \end{pmatrix},$$

and $\mathbf{q}_{2,0}$, $\mu_{2,0}$ and $\boldsymbol{\Omega}_{2,0}$ are obtained by interchanging the labels.

Hence, writing $z_j(u) = F_{1;\mathbf{s}_j}^{\mathbf{W}^{-1}}(u; \lambda_{\mathbf{s}_j})$, $j = 1, 2$, the bivariate copula satisfies, as $q \rightarrow 0$,

$$\begin{aligned} C_2^{\mathbf{W}}(1 - qx_1, 1 - qx_2) &= F_{2;\mathbf{s}_1, \mathbf{s}_2}^{\mathbf{W}}\{z_1(1 - qx_1), z_2(1 - qx_2)\} \\ &\sim 1 - qx_1\Phi_2(\mathbf{q}_{1,0} - \mu_{1,0}; \boldsymbol{\Omega}_{1,0}) - qx_2\Phi_2(\mathbf{q}_{2,0} - \mu_{2,0}; \boldsymbol{\Omega}_{2,0}) \\ &\sim 1 - qx_1\Phi_2[\lambda_{\mathbf{s}_2}^{-1}\{\gamma_{12}/2 + \log(x_1/x_2)\}, -\log q - \lambda_{\mathbf{s}_1}^2/2 - \log x_1; \boldsymbol{\Omega}_{1,0}] \\ &\quad - qx_2\Phi_2[\lambda_{\mathbf{s}_1}^{-1}\{\gamma_{12}/2 + \log(x_2/x_1)\}, -\log q - \lambda_{\mathbf{s}_2}^2/2 - \log x_2; \boldsymbol{\Omega}_{2,0}], \\ &\sim 1 - qx_1\Phi\left(\frac{\sqrt{\gamma_{12}}}{2} + \frac{\log(x_1/x_2)}{\sqrt{\gamma_{12}}}\right) - qx_2\Phi\left(\frac{\sqrt{\gamma_{12}}}{2} + \frac{\log(x_2/x_1)}{\sqrt{\gamma_{12}}}\right), \end{aligned}$$

where $\gamma_{12} = \lambda_{\mathbf{s}_1}^2 - 2\rho(\mathbf{s}_1, \mathbf{s}_2)\lambda_{\mathbf{s}_1}\lambda_{\mathbf{s}_2} + \lambda_{\mathbf{s}_2}^2$. From this, the stable tail dependence function is,

$$\ell(x_1, x_2) = \lim_{q \rightarrow 0} \frac{1}{q} \{1 - C_2^{\mathbf{W}}(1 - qx_1, 1 - qx_2)\} = x_1\Phi\left(\frac{\sqrt{\gamma_{12}}}{2} + \frac{\log(x_1/x_2)}{\sqrt{\gamma_{12}}}\right) + x_2\Phi\left(\frac{\sqrt{\gamma_{12}}}{2} + \frac{\log(x_2/x_1)}{\sqrt{\gamma_{12}}}\right),$$

as required, which corresponds to the dependence structure of the non-stationary Brown-Resnick process (Kabluchko *et al.*, 2009) with variogram γ_{12} .

Furthermore, as the coefficient $\chi_{12}(u) = \Pr\{F_{1;\mathbf{s}_1}^{\mathbf{W}}\{W(\mathbf{s}_1)\} > u \mid F_{1;\mathbf{s}_2}^{\mathbf{W}}\{W(\mathbf{s}_2)\} > u\}$ may be equivalently written as $\chi_{12}(u) = \{1 - 2u + C_2^{\mathbf{W}}(u, u)\}/(1 - u) = 2 - \{1 - C_2^{\mathbf{W}}(u, u)\}/(1 - u)$,

$$\chi_{12} = \lim_{u \rightarrow 1} \chi_{12}(u) = 2 - \ell(1, 1) = 2 - 2\Phi(\sqrt{\gamma_{12}}/2) = 2\{1 - \Phi(\sqrt{\gamma_{12}}/2)\}.$$

For a finite rate parameter $\lambda_{\mathbf{s}} < \infty$, $\mathbf{s} \in \mathcal{S}$, $\gamma_{12} < \infty$, and thus $\chi_{12} > 0$. This implies that the non-stationary model (2.7) is tail-dependent, unless $\lambda_{\mathbf{s}} \rightarrow \infty$. \square

References

- Anderes, E. B. and Stein, M. L. (2011) Local likelihood estimation for nonstationary random fields. *Journal of Multivariate Analysis* **102**(3), 506–520.
- Asadi, P., Davison, A. C. and Engelke, S. (2015) Extremes on river networks. *Annals of Applied Statistics* **9**(4), 2023–2050.
- Blanchet, J. and Davison, A. C. (2011) Spatial modelling of extreme snow depth. *Annals of Applied Statistics* **5**(3), 1699–1725.
- Castro Camilo, D. and de Carvalho, M. (2016) Spectral density regression for bivariate extremes. *Stochastic Environmental Research and Risk Assessment* pp. 1–11.
- Castro Camilo, D., de Carvalho, M. and Wadsworth, J. (2017) Time-varying extreme value dependence with application to leading european stock markets. *Annals of Applied Statistics* To appear.
- Castruccio, S., Huser, R. and Genton, M. G. (2016) High-order composite likelihood inference for max-stable distributions and processes. *Journal of Computational and Graphical Statistics* **25**(4), 1212–1229.
- Cooley, D. S., Naveau, P. and Nychka, D. (2007) Bayesian Spatial Modeling of Extreme Precipitation Return Levels. *Journal of American Statistical Association* **102**(479), 824–840.
- Davison, A. C. and Gholamrezaee, M. M. (2012) Geostatistics of extremes. *Proceedings of the Royal Society A: Mathematical, Physical & Engineering Sciences* **468**(2138), 581–608.
- Davison, A. C., Padoan, S. and Ribatet, M. (2012) Statistical Modelling of Spatial Extremes (with Discussion). *Statistical Science* **27**(2), 161–186.
- Davison, A. C. and Ramesh, N. (2000) Local likelihood smoothing of sample extremes. *Journal of the Royal Statistical Society: Series B (Statistical Methodology)* **62**(1), 191–208.
- de Fondeville, R. and Davison, A. C. (2016) High-dimensional peaks-over-threshold inference for the Brown–Resnick process. Preprint ArXiv:1605.08558.
- Engelke, S., Malinowski, A., Kabluchko, Z. and Schlather, M. (2015) Estimation of Hüsler–Reiss distributions and Brown–Resnick processes. *J. Roy. Statist. Soc. B* **77**, 239–265.
- Ferreira, A. and de Haan, L. (2014) The generalized Pareto process; with a view towards application and simulation. *Bernoulli* To appear.

- Fill, H. D. and Stedinger, J. R. (1995) Homogeneity tests based upon gumbel distribution and a critical appraisal of dalrymple’s test. *Journal of Hydrology* **166**(1-2), 81–105.
- Fischer, E. M. and Knutti, R. (2016) Observed heavy precipitation increase confirms theory and early models. *Nature Climate Change* **6**, 986–991.
- Fuentes, M. (2001) A High Frequency Kriging Approach for Non-Stationary Environmental Processes. *Environmetrics* **12**(5), 469–483.
- Genest, C., Ghoudi, K. and Rivest, L.-P. (1995) A semiparametric estimation procedure of dependence parameters in multivariate families of distributions. *Biometrika* **82**, 543–552.
- Genton, M. G., Johnson, C., Potter, K., Stenchikov, G. and Sun, Y. (2014) Surface boxplots. *Stat* **3**(1), 1–11.
- Gneiting, T., Genton, M. G. and Guttorp, P. (2006) Geostatistical space-time models, stationarity, separability, and full symmetry. *Monographs On Statistics and Applied Probability* **107**, 151.
- Hoerling, M., Eischeid, J., Perlwitz, J., Quan, X.-W., Wolter, K. and Cheng, L. (2016) Characterizing recent trends in U.S. heavy precipitation. *Journal of Climate* **29**(1), 2313–2332.
- Hosking, J. and Wallis, J. (1993) Some statistics useful in regional frequency analysis. *Water resources research* **29**(2), 271–281.
- Hosking, J. R. M. and Wallis, J. R. (2005) *Regional frequency analysis: an approach based on L-moments*. Cambridge University Press.
- Huser, R. and Davison, A. C. (2013) Composite likelihood estimation for the Brown–Resnick process. *Biometrika* **100**(2), 511–518.
- Huser, R. and Davison, A. C. (2014) Space–time modelling of extreme events. *Journal of the Royal Statistical Society: Series B (Statistical Methodology)* **76**(2), 439–461.
- Huser, R., Davison, A. C. and Genton, M. G. (2016) Likelihood estimators for multivariate extremes. *Extremes* **19**(1), 79–103.
- Huser, R. and Genton, M. G. (2016) Non-stationary dependence structures for spatial extremes. *Journal of Agricultural, Biological, and Environmental Statistics* pp. 1–22.
- Huser, R., Opitz, T. and Thibaud, E. (2017) Bridging asymptotic independence and dependence in spatial extremes using gaussian scale mixtures. *Spatial Statistics* **21**, 166–186.
- Huser, R. and Wadsworth, J. L. (2017) Modeling spatial processes with unknown extremal dependence class. Submitted.

- Hüsler, J. and Reiss, R.-D. (1989) Maxima of normal random vectors: between independence and complete dependence. *Statistics & Probability Letters* **7**(4), 283–286.
- IPCC (2014) Climate Change 2014: Synthesis Report. Contribution of Working Groups I, II and III to the Fifth Assessment Report of the Intergovernmental Panel on Climate Change [Core Writing Team, R.K. Pachauri and L.A. Meyer (eds.)]. IPCC, Geneva, Switzerland, 151pp.
- Joe, H. (2014) *Dependence modeling with copulas*. CRC Press.
- Kabluchko, Z., Schlather, M. and De Haan, L. (2009) Stationary max-stable fields associated to negative definite functions. *The Annals of Probability* pp. 2042–2065.
- Krupskii, P., Huser, R. and Genton, M. G. (2016) Factor copula models for replicated spatial data. *Journal of the American Statistical Association* To appear.
- Krupskii, P. and Joe, H. (2015) Structured factor copula models: theory, inference and computation. *Journal of Multivariate Analysis* **138**, 53–73.
- Ledford, A. W. and Tawn, J. A. (1996) Statistics for near independence in multivariate extreme values. *Biometrika* **83**(1), 169–187.
- Lu, L.-H. and Stedinger, J. R. (1992) Sampling variance of normalized gev/pwm quantile estimators and a regional homogeneity test. *Journal of Hydrology* **138**(1-2), 223–245.
- Morris, S. A., Reich, B. J., Thibaud, E. and Cooley, D. (2017) A space-time skew-t model for threshold exceedances. *Biometrics*, to appear. Doi: 10.1111/biom.12644.
- Nychka, D., Wikle, C. K. and Royle, J. A. (2002) Multiresolution Models for Nonstationary Spatial Covariance Functions. *Statistical Modelling* **2**(4), 315–331.
- Opitz, T. (2016) Modeling asymptotically independent spatial extremes based on Laplace random fields. *Spatial Statistics* **16**(1), 1–18.
- Paciorek, C. J. and Schervish, M. J. (2006) Spatial modelling using a new class of nonstationary covariance functions. *Environmetrics* **17**(5), 483–506.
- Padoan, S. A., Ribatet, M. and Sisson, S. A. (2010) Likelihood-based inference for max-stable processes. *Journal of the American Statistical Association* **105**(489), 263–277.
- Reich, B. J., Eidsvik, J., Guindani, M., Nail, A. J. and Schmidt, A. M. (2011) A Class of Covariate-Dependent Spatiotemporal Covariance Functions For The Analysis of Daily Ozone Concentration. *Annals of Applied Statistics* **5**(4), 2465–2487.
- Rootzén, H., Segers, J. and Wadsworth, J. L. (2017) Multivariate generalized Pareto distributions: parameterizations, representations, and properties. Preprint ArXiv:1705.07987.

- Scholz, F. W. and Stephens, M. A. (1987) K-sample anderson–darling tests. *Journal of the American Statistical Association* **82**(399), 918–924.
- Segers, J. (2012) Max-stable models for multivariate extremes. *arXiv preprint arXiv:1204.0332* .
- Sklar, M. (1959) *Fonctions de répartition à n dimensions et leurs marges*. Université Paris 8.
- Stein, M. L. (1999) *Interpolation of Spatial Data: Some Theory for Kriging*. First edition. New York: Springer. ISBN 9780387986296.
- Stein, M. L. (2005) Nonstationary Spatial Covariance Functions. Unpublished.
- Sun, Y. and Genton, M. G. (2012) Functional boxplots. *Journal of Computational and Graphical Statistics* .
- Thibaud, E., Mutzner, R. and Davison, A. C. (2013) Threshold modeling of extreme spatial rainfall. *Water Resources Research* **49**(8), 4633–4644.
- Thibaud, E. and Opitz, T. (2015) Efficient inference and simulation for elliptical Pareto processes. *Biometrika* **102**(4), 855–870.
- Viglione, A., Laio, F. and Claps, P. (2007) A comparison of homogeneity tests for regional frequency analysis. *Water Resources Research* **43**(3).
- Wadsworth, J. L. and Tawn, J. A. (2012) Dependence modelling for spatial extremes. *Biometrika* **99**(2), 253–272.
- Wadsworth, J. L. and Tawn, J. A. (2014) Efficient inference for spatial extreme value processes associated to log-Gaussian random functions. *Biometrika* **101**(1), 1–15.
- Wang, G., Wang, D., Trenberth, K. E., Erfanian, A., Yu, M., Bosilovich, M. G. and Parr, D. T. (2017) The peak structure and future changes of the relationships between extreme precipitation and temperature. *Nature Climate Change* **7**(4), 268–274.
- Westra, S., Alexander, L. V. and Zwiers, F. W. (2013) Global increasing trends in annual maximum daily precipitation. *Journal of Climate* **26**, 3904–3918.
- Westra, S. and Sisson, S. A. (2011) Detection of non-stationarity in precipitation extremes using a max-stable process model. *Journal of Hydrology* **406**(1), 119–128.